SPORE Parachute Design and Selection

Stephanie E. Stout
Georgia Institute of Technology, Atlanta, GA 30332

Eleven parachute types are investigated to determine the best option for the SPORE 1U LEO and 2x2U LEO configurations. The 1U LEO configuration must meet a 5 meters per second impact velocity requirement, and the 2x2U LEO configuration must meet a 40g acceleration limit throughout its trajectory, constraining both the impact deceleration and the parachute opening deceleration due to inflation. The suggested parachute types for the 2x2U LEO configuration are the ringslot, disk-gap-band, extended skirt 14.3% full, and conical ribbon parachutes, due to their low opening forces. The parachute should be deployed at a Mach number less than 0.65 to minimize opening decelerations. However, these designed parachutes do not consistently meet the impact deceleration requirement in a Monte Carlo simulation and should be oversized to account for variability. This strategy is applied to the 1U LEO configuration and results in approximately 49% confidence of meeting the impact velocity requirement with doubling the parachute area. Only 63% confidence is achieved by tripling the parachute area, indicating significantly diminished returns with increasing area. These approximate confidence levels are present with all eleven parachute types.

Table of Contents

Table of Figures

Table of Tables

Nomenclature

a	=	entry vehicle acceleration (m/s^2)
A	=	ballistic parameter
C_d	=	coefficient of drag
C_x	=	infinite mass opening force coefficient
D_0	=	nominal parachute diameter (m)
D_{nose}	=	nose diameter of entry vehicle (m)
F_x	=	maximum canopy opening force (N)
g	=	gravitational constant
m	=	entry vehicle mass (kg)
n	=	fill constant
q	=	dynamic pressure ($kg/m/s^2$)
S	=	parachute area (m^2)
t_f	=	canopy filling time (s)
v_1	=	velocity at line stretch (m/s^2)
V_{impact}	=	entry vehicle impact velocity (m/s^2)
W_t	=	weight of entry vehicle (N)
X_1	=	opening force reduction factor

I. Introduction

The parachute design for the Small Probe for Orbital Return of Experiments (SPORE) is presented in this paper. Two configurations with unique requirements are investigated simultaneously. Eleven parachute types are considered in order to determine the best type or types for each application and down-select for further analysis. The analysis includes parachute sizing, a preliminary opening force investigation using two simple methods, a final opening deceleration investigation, and an impact analysis. The preliminary design and analysis uses methods presented in the Parachute Recovery Systems Design Manual [1]. The final results are obtained using the POST-II (Program to Optimize Simulated Trajectories) trajectory software.

A. SPORE Mission Objective and Requirements

SPORE offers small experiments access to an on-orbit environment and a safe return to Earth for further data analysis [2]. The overall mission concept can be seen in Figure 1. Two sizes of SPORE entry vehicles are designed and are designated “1U” and “2x2U” for the size of the CubeSat payload contained within it. These two vehicle configurations are designed for three orbits: low earth orbit (LEO), geostationary transfer orbit (GTO), and return from the International Space Station (ISS). This analysis targets the 1U LEO and 2x2U LEO combinations, which are designed for thermal protection system and biological or material science payloads, respectively. Since these are very different types of experiments, each configuration has its own driving design requirement related to descent and landing. The 1U LEO configuration requires a 5 meters per second impact velocity, and the 2x2U LEO requires a 40g acceleration limit. This acceleration limit applies to the entire trajectory and will impact not only the landing deceleration, but also the parachute opening deceleration.

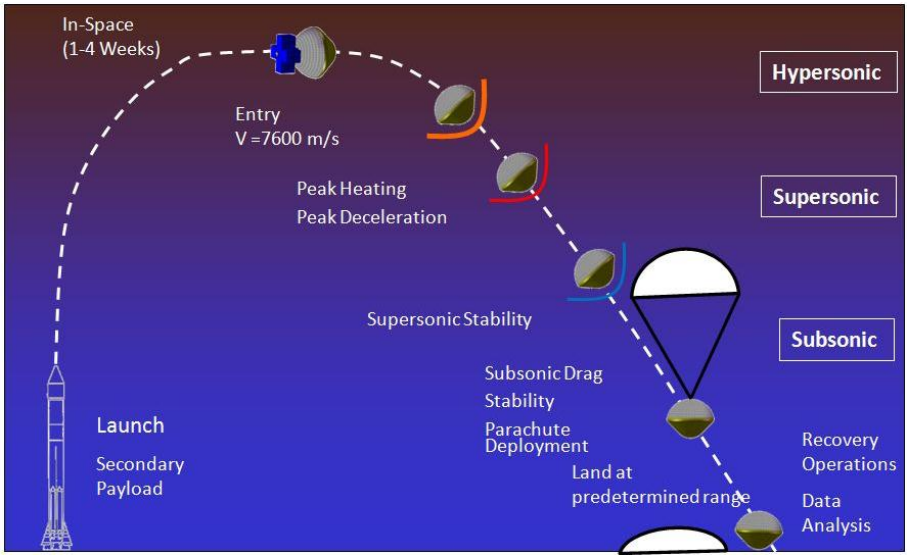

Figure 1 SPORE Mission Concept [2]

B. Entry Vehicle Configurations

Two entry vehicle configurations have been designed for SPORE, based on the geometry of the Mars Microprobe and the interior configuration of Galileo and Pioneer [2]. The 1U configuration supports a single 1U CubeSat payload and the 2x2U configuration contains two 2U CubeSat payloads. The parachute and mortar combination is modeled as a cylinder with an extension and is the same size for both configurations. An overview of each configuration is presented in the following sections.

1. 1U Configuration - TPS

The 1U configuration, pictured in Figure 2 for the TPS payloads, has a diameter of 0.4064 meters and a mass of 7.68 kilograms, neglecting the parachute and mortar. The location of the center of gravity and the moments are inertia for this configuration are in Table 1. The coordinate system for these, intended for the POST inputs, can be seen in Figure 3.

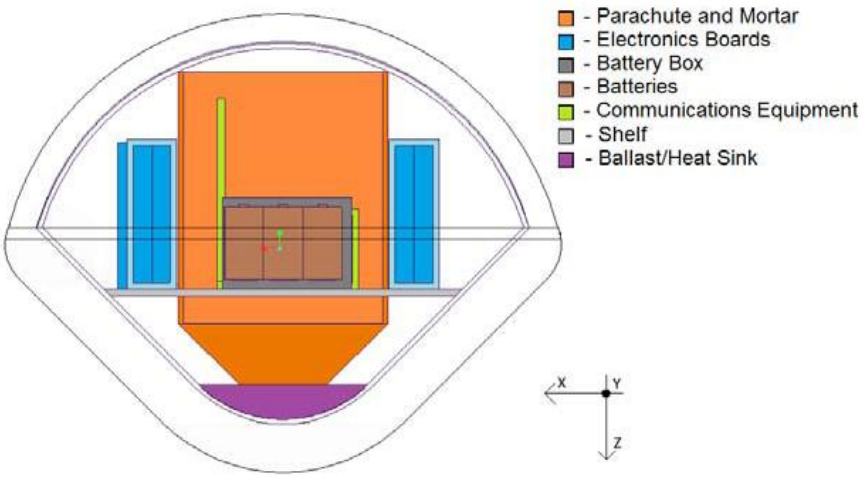

Figure 2 1U Configuration Model [2]

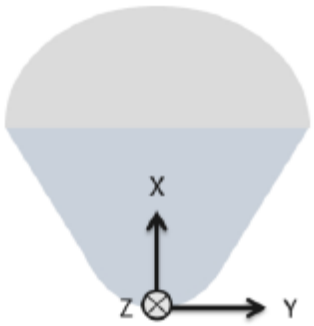

Figure 3 Coordinate System for POST inputs [3]

Table 1 Center of Gravity Location and Moments of Inertia for 1U [3]

CG_x (mm)	143.303	I_{xx}	0.1
CG_y (mm)	2.743	I_{yy}	0.082
CG_z (mm)	-1.89	I_{zz}	0.089

2. 2x2U Configuration – BIO/MSE

The 2x2U configuration, pictured in Figure 4 for the biological and materials science payloads, has a diameter of 0.6505 meters and a mass of 28.67 kilograms, neglecting the parachute and mortar. The location of the center of gravity and the moments are inertia for this configuration are in Table 2.

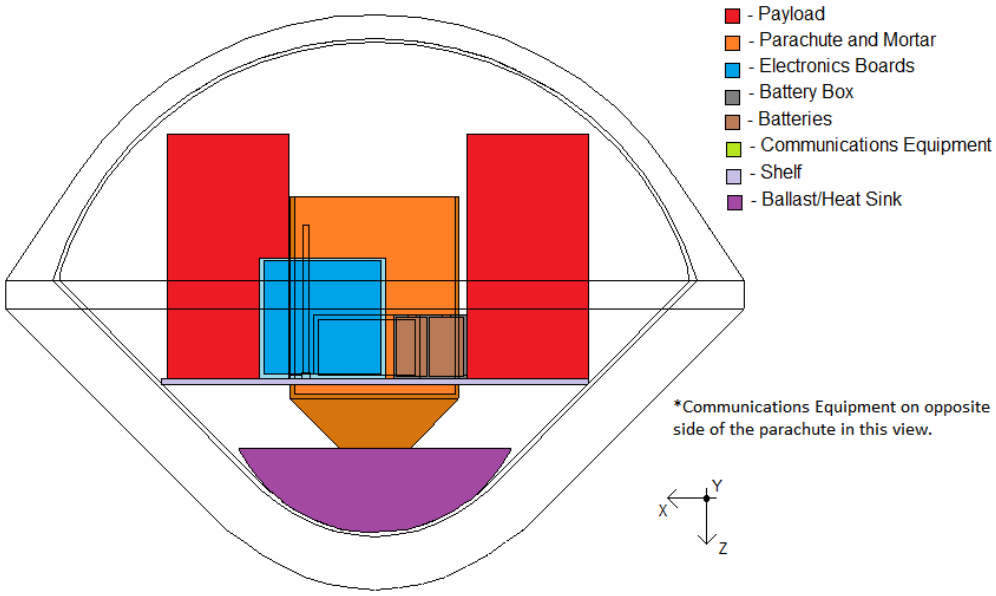

Figure 4 2x2U Configuration Model [2]

Table 2 Center of Gravity Location and Moments of Inertia for 2x2U [3]

CG_x (mm)	245.275	I_{xx}	0.717
CG_y (mm)	2.872	I_{yy}	0.611
CG_z (mm)	-1.047	I_{zz}	0.649

C. Descent and Landing

The targeted landing site is the Woomera Prohibited Area in Australia, due to its remote location, restricted airspace, and history as a test facility for hypersonic vehicles and other aerospace programs [4]. Additionally, there is heritage as a re-entry vehicle landing site, as the Japanese Hayabusa Sample Return

Capsule landed there in June 2010. Table 3 presents the re-entry trajectory parameters determined by Nicole Bauer [3] in order to target this landing site.

Table 3 Baseline Entry Trajectories [3]

Configuration	1U LEO	2x2U LEO
Radius (km)	6503.1	6503.1
Longitude (°E)	137.65	137.59
Latitude (°N)	-16.65	-14.85
Velocity (m/s)	7780	7780.5
Gamma (°)	-5	-5.04
Azimuth (°)	182.9	182.9

The parachute will be deployed subsonically by a mortar. While the parachute is sized the meet the deceleration limits at impact, the deceleration due to deployment must also be investigated. Due to the small masses of these systems and the stringent maximum acceleration requirement, opening deceleration caused by parachute inflation is a particular concern. The snatch force at suspension line stretch should be determined, but it is typically less than the opening force [5]. A finite mass condition is assumed in this analysis because of the low canopy loading, $W/(C_D S)_p$, experienced by the parachutes. This results in velocity decay during inflation and lower opening forces than under infinite mass conditions [1]. Additionally, the maximum opening force will occur prior to full inflation.

The final deployment mach number and altitude selection will be determined from the trajectory and the opening deceleration profile.

II. Parachute Sizing

The following describes the prodecure to appropriately size a parachute based on the desired impact velocity. Since the requirement for the 2x2U configuration is described by acceleration, impact velocity is translated to impact deceleration using Meyer's Theory. Equation 1 shows this relationship between impact velocity and deceleration [6], assuming a small penetration at impact. Once the impact velocity is found from the maximum impact deceleration, the calculations for the 1U and 2x2U configurations are the same.

Equation 1

$$a = V_{impact}\sqrt{\frac{D_{nose}}{m}}$$

The required C_dS of the parachute is found by rearranging the drag force equation in Equation 2, using the system mass and the atmospheric density at impact. The atmospheric density for a landing site at the Woomera Prohibited Area is 1.205 kg/m^3. The required parachute area can then be determined by dividing the C_dS by the C_d of the selected parachute type. Table 4 presents the values of Cd used in this analysis, which are an average of the ranges suggested by Knacke for each parachute type [1]. Table 4 also includes other parameters of interest in this investigation, where n is the fill constant and C_x is the infinite mass opening force coefficient.

Equation 2

$$C_d S = \frac{m g_E}{\frac{1}{2}\rho {V_{impact}}^2}$$

Table 4 Parameters by Parachute Type

Parachute Type	C_d	n	C_x
Conical	0.825	8	1.8
Biconical	0.835	8	1.8
Triconical	0.88	8	1.8
Extended Skirt 10% Flat	0.825	10	1.4
Extended Skirt 14.3% Full	0.825	12	1.4
Annular	0.9	9	1.4
Cross	0.725	8.7	1.15
Conical Ribbon	0.525	8	1.05
Ringslot	0.605	14	1.05
Ringsail	0.8	7	1.1
Disk-Gap-Band	0.55	10	1.3

Finally, the nominal diameter of the parachute can be calculated using Equation 3.

Equation 3

$$D_0 = \sqrt{\frac{4S}{\pi}}$$

Table 5 and Table 6 present the results of the parachute sizing calculations for each of the eleven parachute types. The triconical and annular parachutes require the smallest area due to their large C_d, while the conical ribbon, disk-gap-band, and ringslot parachutes require the largest area.

Table 5 2x2U Calculated Parachute Size

Parachute Type	Required Area (m^2)	Nominal Diameter (m)
Conical	25.67	5.72
Biconical	25.36	5.68
Triconical	24.06	5.54
Extended Skirt 10% Flat	25.67	5.72
Extended Skirt 14.3% Full	25.67	5.72
Annular	23.53	5.47
Cross	29.21	6.10
Conical Ribbon	40.33	7.17
Ringslot	35.00	6.68
Ringsail	26.47	5.81
Disk-Gap-Band	38.50	7.00

Table 6 1U LEO Calculated Parachute Size

Parachute Type	Required Area (m^2)	Nominal Diameter (m)
Conical	6.06	2.78
Biconical	5.99	2.76
Triconical	5.68	2.69
Extended Skirt 10% Flat	6.06	2.78
Extended Skirt 14.3% Full	6.06	2.78
Annular	5.56	2.66
Cross	6.90	2.96
Conical Ribbon	9.53	3.48
Ringslot	8.27	3.24
Ringsail	6.25	2.82
Disk-Gap-Band	9.09	3.40

III. Preliminary Opening Force Investigation

Two methods suggested by Knacke [1] were utilized to provide an estimation of the maximum opening force. The $W/(C_DS)$ method uses a correlation derived from wind tunnel tests to relate the steady-state drag with the maximum opening force. The Pflanz method is somewhat more accurate than the $W/(C_DS)$ method and is mathematically exact [1]. It assumes a horizontal flight path, and so 1g needs to be added to to the opening deceleration to account for a vertical flight path. This method takes into account both the weight and velocity of the entry vehicle and the predicted inflation time and inflation profile of the parachute.

A. $W/(C_DS)$ Method

This method correlates the steady-state drag force with the maximum opening force through the infinite mass opening force coefficient, Cx, as seen in Equation 4. Since this investigation concerns finite mass inflation, an opening force reduction factor, X1, is required.

Equation 4

$$F_x = (C_D S)_p q C_x X_1$$

The Cx for each parachute type was listed in Table 4. In this method, X1 is determined using the canopy loading and Figure 5. The small masses of the entry vehicle would require extrapolation on the left side of the curve, resulting in a very small X1 and therefore a small maximum opening force. However, this is unrealistic and a more precise method must be considered.

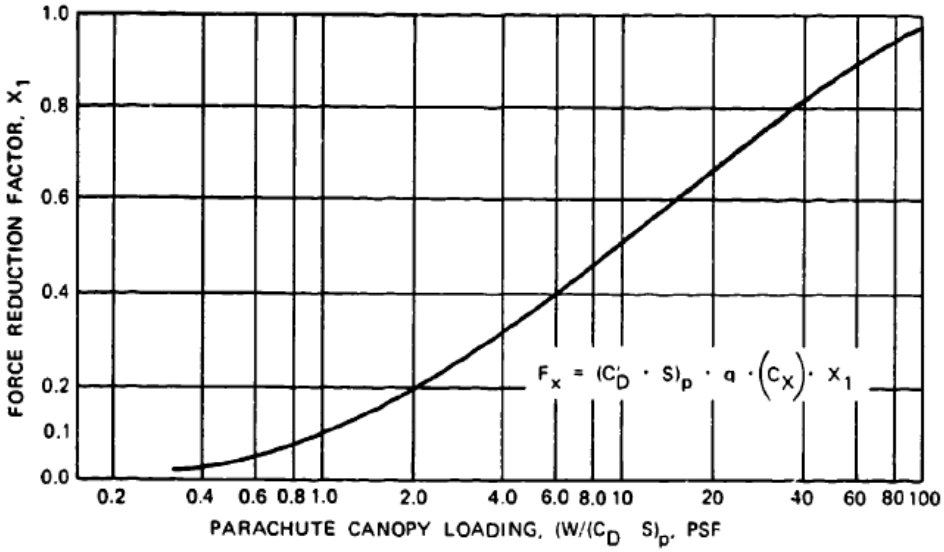

Figure 5 Opening Force Reduction Factor vs Parachute Canopy Loading [1]

B. Pflanz Method

In this method, the ballistic parameter, A, is calculated using Equation 5 where v1 is the velocity at line stretch and tf is the inflation time. The inflation time can be calculated using Equation 6.

Equation 5

$$A = \frac{2W_t}{(C_D S)_p \rho g v_1 t_f}$$

Equation 6

$$t_f = \frac{nD_0}{v_1}$$

Once the ballistic parameter is found, Figure 6 can be used to determine X1, which is then plugged into Equation 4 to determine the maximum opening force. The n=1 curve is intended for conical ribbon and ringslot parachutes, and the n=2 curve is for the conical, biconical, triconical, and extended skirt parachutes [1]. Knacke does not list a correlation for annular, cross, ringsail, and disk-gap-band parachutes.

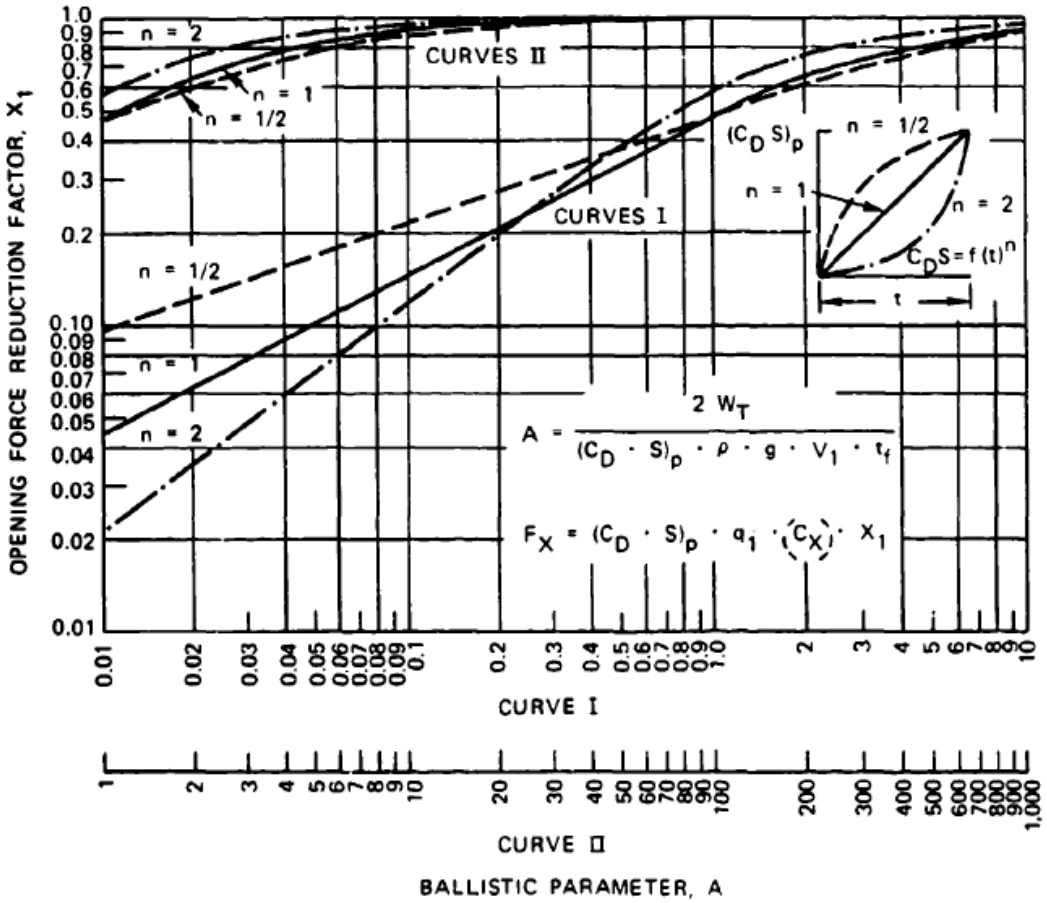

Figure 6 Ballastic Parameter vs Opening Force Reduction Factor [1]

The results from the Pflanz Method calculations are presented in Table 7 and Table 8. These calculations assumed a deployment altitude of 5 kilometers and used the trajectory results from Bauer's POST analysis [3]. This resulted in a deployment Mach number of 0.5 for the 2x2U configuration (LEO and GTO assumed the same due to simplicity of the calculation) and 0.48 for the 1U-LEO configuration. Using this method, all of the parachutes analyzed exceed the maximum allowed acceleration of 40g for the 2x2U configurations. According to experts at Pioneer Aerospace, the Pflanz method tends to overpredict opening force, and so another method will need to be employed to determine with greater fidelity the opening deceleration. These results do show that the extended skirt parachutes, the conical ribbon parachute, and the ringslot parachute lead to much smaller opening decelerations than the conical family of parachutes. While the 40g limit is not a requirement for the 1U-LEO configuration, it is interesting to note that it has a significantly larger opening deceleration using this method than the 2x2U configurations.

Table 7 2x2U Pflanz Method Calculations and Results

Parachute Type	Required Area (m^2)	Nominal Diameter (m)	Filling Time (s)	Ballistic Parameter	Opening Deceleration (g)
Conical	25.67	5.72	0.32	0.06	121.8
Biconical	25.36	5.68	0.32	0.06	121.8
Triconical	24.06	5.54	0.31	0.06	122
Extended Skirt 10% Flat	25.67	5.72	0.4	0.05	82.9
Extended Skirt 14.3% Full	25.67	5.72	0.48	0.04	71
Conical Ribbon	40.33	7.17	0.67	0.03	69.8
Ringslot	35.00	6.68	0.66	0.03	70.2

Table 8 1U-LEO Pflanz Method Calculations and Results

Parachute Type	Required Area (m^2)	Nominal Diameter (m)	Filling Time (s)	Ballistic Parameter	Opening Deceleration (g)
Conical	6.06	2.78	0.14	0.19	203.6
Biconical	5.99	2.76	0.14	0.2	203.7
Triconical	5.68	2.69	0.14	0.2	214.1
Extended Skirt 10% Flat	6.06	2.78	0.18	0.16	126.7
Extended Skirt 14.3% Full	6.06	2.78	0.22	0.13	110.9
Conical Ribbon	9.53	3.48	0.18	0.16	105.5
Ringslot	8.27	3.24	0.29	0.1	88.4

IV. Final Opening Deceleration Investigation – 2x2U LEO

POST-II, or Program to Optimize Simulated Trajectories, is used for the remaining opening deceleration analysis, as well as the impact analysis.

A. Model Development

The POST model used in this analysis is based on the model created by Bauer [3], with an added parachute inflation event. The parachute drag option is turned on at the selected deployment Mach number and inflates until the nominal parachute diameter is reached. The parachute drag option without inflation remains selected until impact. The POST inflation factor is assumed to be the fill constant indicated by Knacke [1].

Two baseline models are used to complete the analysis. The first, used for the parachute type selection, is a basic trajectory model whose inputs do not include variation. This results in repeatable outputs from POST. The second model is a Monte Carlo model that includes input variation as well as a wind model.

B. Parachute Type Selection

Each of the 11 parachute types is investigated using the model described above. The deployment Mach number is varied from 0.5 to 0.8, and the resulting maximum accelerations are listed in Table 9. The shaded portions indicate the combinations of parachute type and deployment mach number that result in maximum accelerations under the 40g limit. Several notions emerge from the mach number sweep. The first is that every parachute type has acceptable maximum accelerations for the mach number range of 0.5 to 0.59. The second is that there is not a monotonic trend with increasing mach number. The shading indicates that even after the 40g threshold is exceeded as the mach number increases, there are larger mach numbers that also produce maximum accelerations under the limit.

Table 9 Opening Deceleration (g) Results of Mach Number Sweep

Mach	*Conical*	*Bi-conical*	*Tri-conical*	*Extended Skirt 10%*	*Extended Skirt 14.3%*	*Conical Ribbon*	*Ringslot*	*Ringsail*	*DGB*	*Annular*	*Cross*
0.5	34.43	34.29	33.66	32.16	29.90	33.37	22.99	36.02	28.57	32.48	33.74
0.51	34.73	34.63	34.11	32.05	29.43	31.11	21.05	36.45	26.42	32.83	33.63
0.52	34.40	34.31	33.94	31.53	28.74	30.14	20.07	36.14	25.45	32.58	33.05
0.53	27.70	27.62	27.11	26.97	26.06	28.87	22.54	28.68	26.34	26.78	27.44
0.54	28.15	28.16	28.14	27.03	25.83	28.62	22.26	30.62	26.10	27.69	27.38
0.55	27.98	28.28	29.59	26.80	25.94	27.10	23.47	34.21	25.81	27.14	27.13
0.56	30.18	30.47	31.64	26.75	26.01	27.27	22.44	36.53	25.07	26.32	27.31
0.57	29.87	29.90	31.19	22.62	23.35	27.62	24.16	35.59	26.33	27.87	24.51
0.58	33.34	33.31	33.20	30.25	27.30	29.70	19.28	35.58	25.00	31.80	31.63
0.59	35.87	35.97	36.31	30.77	26.32	25.61	21.49	38.50	22.03	34.12	32.41
0.6	41.31	41.55	42.49	30.47	26.53	28.04	24.12	47.79	26.55	37.03	34.02
0.61	43.61	43.87	44.82	32.74	26.79	28.68	24.44	50.07	26.95	39.38	36.29
0.62	44.53	44.99	46.94	33.93	28.07	29.13	23.09	50.17	26.49	41.63	36.70
0.63	37.40	37.29	37.36	30.71	25.09	36.63	24.74	41.57	27.94	34.47	34.00
0.64	36.85	37.02	37.71	30.99	28.06	31.11	20.41	39.96	26.36	34.84	32.80
0.65	37.19	37.34	37.99	31.89	27.40	38.08	22.59	40.09	29.92	35.31	33.58
0.66	45.29	45.19	44.77	37.91	31.63	41.41	26.13	49.93	33.00	41.16	41.42
0.67	37.51	37.65	38.22	32.38	28.56	33.23	21.43	40.06	27.47	35.86	34.15
0.68	55.16	55.37	56.33	44.68	36.77	37.23	26.75	61.05	31.86	51.27	47.97
0.69	56.08	56.31	57.04	45.94	38.16	39.38	27.29	61.84	33.63	52.15	49.33
0.7	54.15	54.20	54.01	45.78	38.79	44.63	27.71	58.87	37.24	50.02	49.25
0.71	51.67	52.27	54.89	42.75	36.23	33.16	24.92	55.76	29.23	50.62	44.26
0.72	37.02	37.12	37.63	33.27	29.89	34.11	24.35	38.84	31.82	36.43	34.57
0.73	59.64	59.86	60.28	50.21	42.71	45.02	29.73	65.09	38.60	55.90	53.54
0.74	36.53	36.62	36.97	33.20	30.17	37.42	27.64	38.12	35.42	35.48	34.37
0.75	47.86	48.53	51.52	41.01	35.89	33.06	25.01	50.31	29.91	48.37	41.46
0.76	46.21	45.80	44.31	47.22	42.95	52.67	34.11	46.98	44.61	43.87	48.69
0.77	36.10	35.89	35.87	35.76	35.96	50.80	33.97	36.93	43.85	34.64	36.93
0.78	48.76	49.46	52.66	41.97	37.02	32.48	28.18	51.14	30.56	49.57	42.20
0.79	53.85	54.63	57.78	45.63	39.79	32.22	27.44	57.32	29.75	53.92	46.32
0.8	65.51	65.75	64.93	55.55	47.99	43.25	33.06	68.57	39.19	62.26	58.37

Several parachute types appear to be better than the others in that the majority of the deployment mach numbers investigated result in acceptable maximum accelerations. The best parachute types are ringslot, disk-gap-band, extended skirt 14.3%, and conical ribbon, which confirms the trend seen in the preliminary analysis using the Pflanz method. The ringslot parachute has acceptable opening decelerations for the entire Mach number regime. The deployment mach number for each type is selected from the minimum deceleration from Table 9. Table 10 displays the selected deployment mach numbers for each of these four selected parachute types and the required parachute size. The extended skirt 14.3% full parachute offers similar performance with a much smaller parachute.

Table 10 Selected Parachute Types

	Ringslot	DGB	Extended Skirt 14.3%	Conical Ribbon
Parachute Area (m^2)	35.0	38.5	25.7	40.3
Parachute Diameter (m)	6.68	7.00	5.72	7.17
Deployment Mach Number	0.58	0.59	0.57	0.59
Deployment Altitude (m)	12,336	12,930	15,146	12,922
Maximum Acceleration (g)	19.28	20.03	23.35	25.61

The following charts explore the details behind these results for the ringslot parachute. The other selected parachutes show similar trends. Figure 7 illustrates that there is not a monotonic trend with increasing Mach number. The curves plotted ranges from Mach number 0.5 to 0.8 and are in increments of 0.05. The curves are overlaid prior to the spike at inflation, confirming that they follow the same trajectoriy. As the deployment Mach number increases, the scenario time of deployment decreases, since higher Mach numbers occur earlier in the trajectory. It is apparent that the larger deployment Mach number result in significantly higher opening decelerations than smaller deployment Mach numbers.

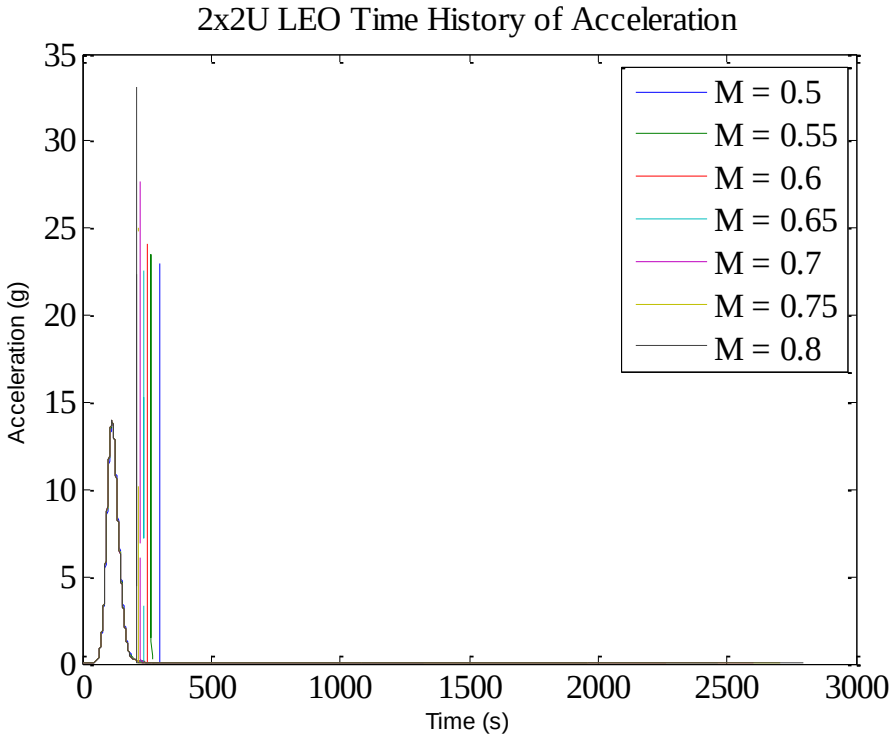

Figure 7 Ringslot Time History of Acceleration for Varied Mach Numbers

Figure 8 plots the deployment altitude, dynamic pressure, and the resulting inflation time to explain the behavior in Figure 7. The relationship between the deployment mach number and deployment altitude is not linear, resulting in significant variations in altitude for small changes at lower Mach numbers. For instance, the difference in altitude from 0.5 to 0.55 Mach is approximately 4900 meters while the difference from 0.75 to 0.8 Mach is only about 1850 meters. This results in significant difference in dynamic pressure at deployment and inflation, which directly affects the time to full inflation. The dynamic pressure and inflation time curves are almost identical, except that the dynamic pressure has a slightly greater slope throughout the Mach number regime. The dynamic pressure and the inflation time curves are fairly linear with a small slope from Mach 0.65 to Mach 0.8, but have curvature with very large slopes at Mach numbers less than 0.65.

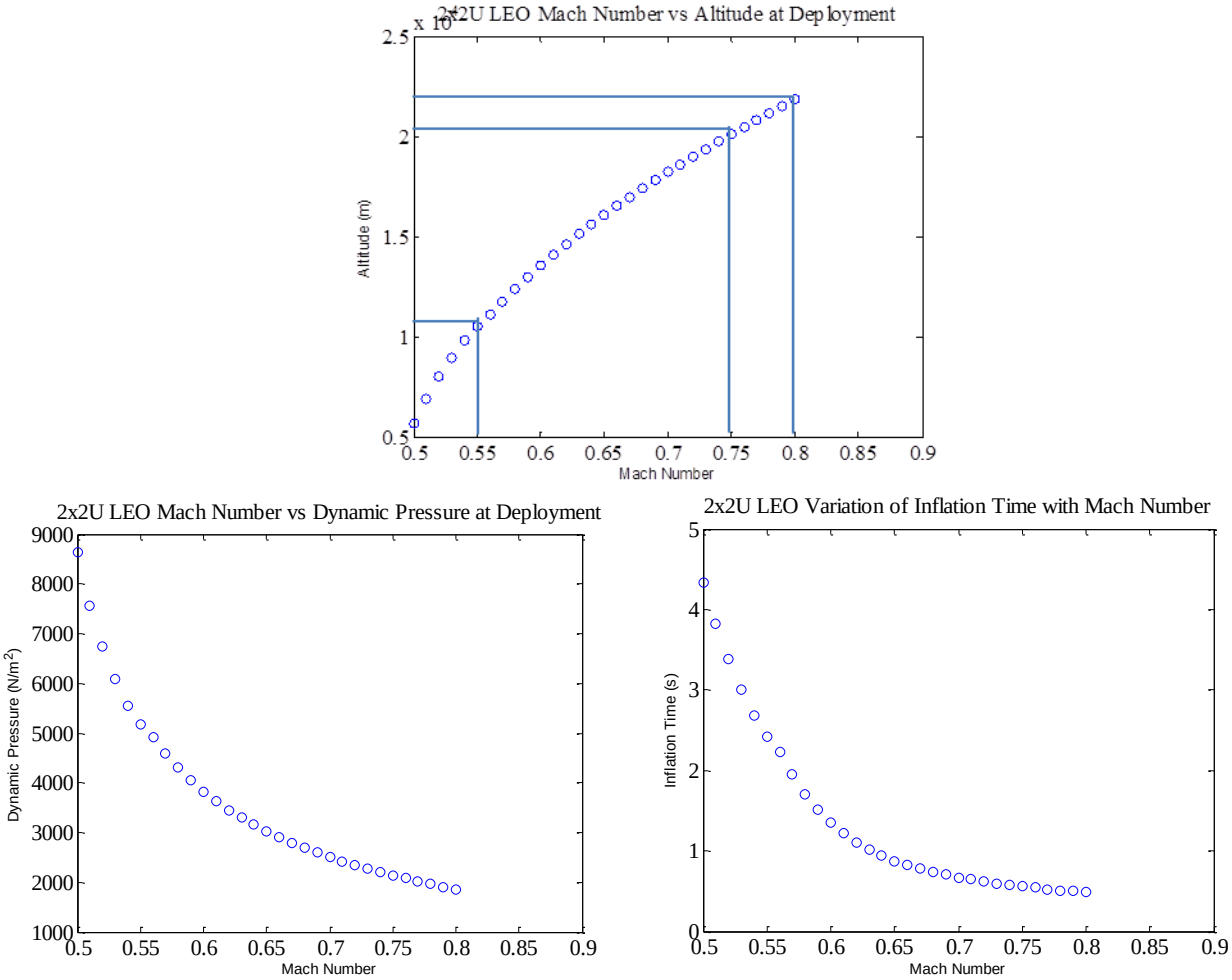

Figure 8 Ringslot Altitude, Dynamic Pressure, Inflation Time Variation with Mach Number

Additionally, Figure 8 indicates that the parachutes experience much larger inflation times at lower Mach numbers. Figure 9 plots the deceleration with respect to inflation time, dynamic pressure, and mach number, and shows the general trend that larger inflation times result in smaller opening decelerations. Very small inflation times (less than one second), result in much larger decelerations. However, there does not appear to be much reduction in deceleration for increasing the inflation time from one second to four seconds. These results are grouped between 20 and 25g decelerations. An inflation time of one second roughly corresponds to a deployment Mach number of 0.65. Therefore it is desirable to target Mach numbers less than 0.65 to take advantage of the larger inflation times and smaller resulting opening decelerations.

Like the charts above, the dynamic pressure versus maximum acceleration shows virtually identical trends as the inflation time versus maximum acceleration chart. The Mach number versus maximum acceleration chart reiterates that the maximum acceleration increases with increasing Mach number. Mach numbers greater than 0.65 indicate a trend with a larger slope than at smaller Mach numbers, resulting in greater variations in maximum acceleration.

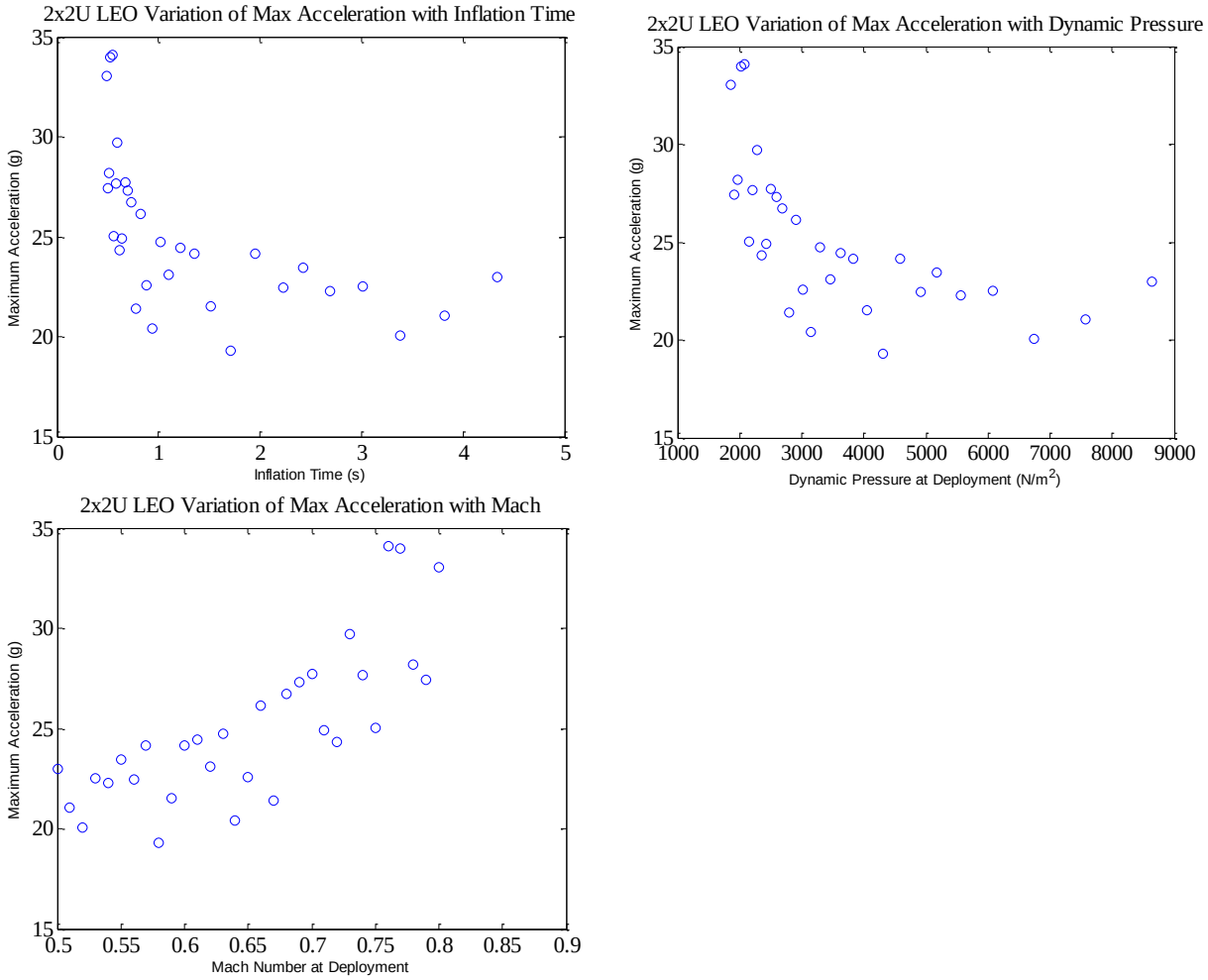

Figure 9 Ringslot Opening Deceleration Variation with Inflation Time, Dynamic Pressure, and Mach Number

C. 2x2U Monte Carlo Simulation Results

The selected parachutes discussed above are used in a Monte Carlo simulation to determine the confidence that the maximum opening deceleration will be under the allowed 40g limit. Two hundred runs are conducted for each of the selected parachutes. The results from the Monte Carlo simulations can be seen in Appendices A through D. These results feature histograms of the maximum opening acceleration, the percent of the parachute that is inflated at the maximum acceleration, the time to full inflation, and the dynamic pressure at inflation. All of the 200 runs for each of the selected parachutes result in acceptable opening decelerations.

Table 11 presents the statistics of the results of the Monte Carlo simulation. The ringslot parachute demonstrates the lowest average opening deceleration of the selected four parachutes, as well as the smallest standard deviation. This parachute also has the largest average inflation time. The standard deviation is very small in general for the inflation time. The disk-gap-band and extended skirt 14.3% full parachutes show a maximum acceleration peak that is shifted to the right of the distribution, indicating a tendency towards larger maximum accelerations. The ringslot and conical ribbon parachutes result in maximum acceleration peaks that are approximately at the center of the distribution, though the conical ribbon parachute has a much wider peak.

The variation in the mean dynamic pressure between the four parachutes is due to the different deployment conditions. The maximum deceleration occurs very early in the inflation process, when the parachutes are approximately 0.1% inflated. This is due to the finite mass inflation [1].

Table 11 Inflation Statistics

	Ringslot	DGB	Extended Skirt 14.3%	Conical Ribbon
Deployment Mach Number	0.58	0.59	0.57	0.59
Deployment Altitude (m)	12,336	12,930	15,146	12,922
Mean Maximum Deceleration (g)	21.207	24.657	24.077	27.399
Standard Deviation Max Deceleration	1.705	1.757	2.195	2.13
Mean Dynamic Pressure (N/m^2)	4289.2	4048.6	4534	4055.6
Standard Deviation Dynamic Pressure	21.318	13.725	19.808	13.954
Mean Inflation Time (s)	1.705	0.85	1.027	0.591
Standard Deviation Inflation Time	0.09	0.0317	0.05	0.0173
Mean % Inflated at Max Deceleration	0.131	0.121	0.094	0.123

V. Impact Investigation

A. 2x2U LEO Impact Deceleration

A Monte Carlo investigation into the impact deceleration revealed that the parachute would need to be oversized from the original design in order to ensure that the impact deceleration remains within the allowable 40g limit. With the original parachute design, the ringslot parachute resulted in only acceptable impact decelerations only 1.5% of the time, while the other parachutes resulted in 3%, 4%, and 1.5% for the disk-gap-band, extended skirt 14.3% and conical ribbon parachutes, respectively. The histograms for impact velocity and impact deceleration for each parachute are featured in Appendix E. Table 12 presents the mean and standard deviation for each. The impact characteristics are very similar between the different parachutes.

Table 12 Impact Statistics

	Ringslot	DGB	Extended Skirt 14.3%	Conical Ribbon
Mean Impact Velocity (m/s)	6.245	6.246	6.218	6.26
Standard Deviation Impact Velocity	1.152	1.153	1.163	1.148
Mean Impact Deceleration (g)	52.215	52.133	52.231	52.2
Standard Deviation Impact Deceleration	9.6326	9.627	9.7704	9.576

B. 1U LEO Impact Velocity

Since accelerations are not a stated requirement for the 1U LEO vehicle, no opening deceleration analysis was conducted to determine the optimum deployment Mach number. However, since accelerations would ideally be minimized the deployment Mach number for the 1U LEO vehicle was selected to be 0.5 Mach, with the reasoning that opening decelerations are smaller at lower Mach numbers. A Monte Carlo simulation is run for each of the eleven parachute types at the baseline design for each. The results revealed that the impact velocity remained under 5 meters per second for only 1 to

4.5% of the runs. This is the same problem seen with the 2x2U LEO impact deceleration.Therefore, the parachutes were increased in size to better meet the requirement. Table 13 shows the results through 300% of the baseline areas for the biconical, extended skirt 14.3% full, and ringsail parachutes. These were selected because they had the highest confidence at 100% parachute area. There is a significant increase in confidence for 150% area, but the increases drop off as parachute area increases. At triple the original area, there is still only 63% confidence that the configuration will result in acceptable impact velocities.

Table 13 Confidence with Varied Parachute Area

	Size	Biconical	Extended Skirt 14.3%	Ringsail
Confidence	100%	0.025	0.035	0.045
	150%	0.33	0.33	0.32
	200%	0.48	0.485	0.49
	250%	0.57	0.55	0.57
	300%	0.63	0.63	0.63
Parachute Area	100%	6.498	6.265	6.465
	150%	9.747	9.520	9.828
	200%	12.995	12.848	13.270
	250%	16.050	16.256	16.796
	300%	19.493	19.747	20.411
Parachute Diameter	100%	2.876	2.824	2.869
	150%	3.523	3.482	3.538
	200%	4.068	4.045	4.110
	250%	4.521	4.550	4.625
	300%	4.982	5.014	5.098

Table 14 presents the impact velocity results for all of the parachute types for 100% and 300% parachute area. The histograms for impact velocity, opening deceleration, and dynamic pressure at inflation are located in Appendices F and G. The resulting performance is very similar between the parachutes, and the most largest difference is in the parachute size to obtain that perforamce. For 300% parachute area, each parachute results in approximately 63% confidence with an average impact velocity of 4.88 meters per second and a standard deviation of 1.41.

The 100% area parachutes demonstrate reasonable opening decelerations. Many of them range from 30g to 65g, peaking around 45g or 50g. The ringsail parachute indicates the worst behavior, ranging from 45g to 75g, peaking around 55g. The ringslot, disk-gap-band, and extended skirt 14.3% full parachutes, like in the previous analysis, provide the best opening decelerations, remaining under 40g.

The 300% area parachutes result in generally lower opening decelerations, and the distributions are shaped such that two peaks are indicated. Most of the parachutes range from 20g to 55g, with peaks at 25g and 50g. In this analysis, the extended skirt 14.3% full and the disk-gap-band parachutes emerge as the best for opening decelerations, with a distribution from 20g to 40g and peaks at 25g and 35g.

Table 14 Impact Velocity Statistics

	Size	Conical	Bi-conical	Tri-conical	Extended Skirt 10%	Extended Skirt 14.3%	Annular	Cross	Conical Ribbon	Ringslot	Ringsail	DGB
Confidence (%)	100%	2.5	2.5	2.5	2	3.5	2.5	1	2.5	2	4.5	2.5
	300%	62.5	63	63	62.5	63	63	63	63	62.5	63	62.5
Mean Impact Velocity (m/s)	100%	6.419	6.429	6.429	6.42	6.424	6.42	6.424	6.428	6.422	6.438	6.428
	300%	4.883	4.882	4.881	4.881	4.884	4.882	4.885	4.881	4.88	4.884	4.88
SD Impact Velocity	100%	1.13	1.121	1.117	1.119	1.135	1.127	1.211	1.114	1.119	1.125	1.122
	300%	1.413	1.413	1.414	1.409	1.414	1.411	1.411	1.41	1.416	1.414	1.413
Parachute Area (m^2)	100%	6.265	6.498	5.865	6.265	6.265	5.732	7.125	9.99	8.626	6.465	9.52
	300%	19.747	19.493	18.428	19.747	19.747	17.991	22.546	32.406	25.878	20.411	30.732
Parachute Diameter (m^2)	100%	2824	2.876	2.733	2.824	2.824	2.701	3.012	3.567	3.312	2.869	3.482
	300%	5.014	4.521	4.844	5.014	5.014	4.786	5.358	6.424	5.740	5.098	6.255

1. Effect of Varied Mass

The mass of the entry vehicle is changed to investigate the effect of mass on the final confidence level for impact velocity. A 5kg and a 12kg entry vehicle are studied, and the initial results indicate that there is not a correlation between mass and the confidence level. Both the masses result in 2.5% confidence for 100% parachute area and 48% confidence for 200% area. This is presented in Table 15 and Table 16.

Table 15 Confidence with 5kg Entry Vehicle

Ringsail 5kg	100%	200%
Entry Mass w/ Parachute (kg)	5.2022	5.3374
Parachute Area (m2)	4.2297	8.6861
Parachute Diameter (m)	2.3207	3.3256
Confidence	0.025	0.48
Average Impact Velocity (m/s)	6.4363	5.3227

Table 16 Confidence with 12kg Entry Vehicle

Ringsail 12kg	100%	200%
Entry Mass w/ Parachute (kg)	12.379	12.69
Parachute Area (m2)	10.067	20.653
Parachute Diameter (m)	3.5801	5.128
Confidence	0.025	0.475
Average Impact Velocity (m/s)	6.4177	5.3186

VI. Conclusion

The results of the opening deceleration analysis for the 2x2U configuration recommend the use of either the ringslot, disk-gap-band, extended skirt 14.3% full, or conical ribbon parachutes. These follow the general trend that parachutes with lower C_d result in a smaller opening force, while requiring a larger parachute. The extended skirt 14.3% full parachute offers performance comparable to the other recommended parachutes while requiring a significantly smaller area. For 200 runs in a Monte Carlo

simulation, each of these recommended parachute types meet the 40g deceleration requirement every time. Furthermore, the results indicate that the ideal deployment Mach number for this configuration is less than 0.65 Mach to minimize the opening decelerations. Additional analysis reveals that these selected parachutes for the 2x2U configuration do not meet the deceleration requirement with high confidence in a Monte Carlo simulation, implying that the parachute needs to be oversized to account for variability.

With this in mind, the parachutes for the 1U configuration are increased in area to determine how large the parachutes would need to be to result in high confidence of meeting the 5 meters per second impact velocity requirement. The Monte Carlo simulations reveal approximately 2% confidence at 100% area, 49% at double the area, and only 63% at triple the area, indicating significantly diminished returns with increasing area. These trends are seen in all eleven of the parachutes investigated, and a brief analysis indicates that varying the mass of the entry vehicle does not have a significant effect.

Bibliography

[1] T. W. Knacke, Parachute Recovery Systems Design Manual, China Lake, CA: Naval Weapons Center, 1991.

[2] "Small Probes for Orbital Return of Experiments (SPORE) Final Report," Aurora Flight Sciences and Georgia Tech Center for Space Systems, 2012.

[3] N. Bauer, "SPORE Mission Design," Georgia Institute of Technology, Atlanta, GA, 2012.

[4] I. R. Tuohy, "Advantages of the Woomera Test Facility for Hypersonic Flight Programs," in *14th AIAA/AHI Space Planes and Hypersonic Systems and Technologies Conference*, 2006.

[5] E. J. Fallon and R. Sinclair, "Design and Development of the Main Parachute for the Beagle 2 Mars Lander," in *17th AIAA Aerodynamic Decelerator Systems Technology Conference and Seminar*, Monterey, CA, 2003.

[6] R. A. Mitcheltree, S. Kellas, J. T. Dorsey, D. P. N and C. J. Martin, "A Passive Earth-Entry Capsule for Mars Sample Return," *American Institute of Aeronautics and Astronautics*, 1998.

Appendix A – Ringslot Parachute Inflation Monte Carlo Results – 2x2U LEO

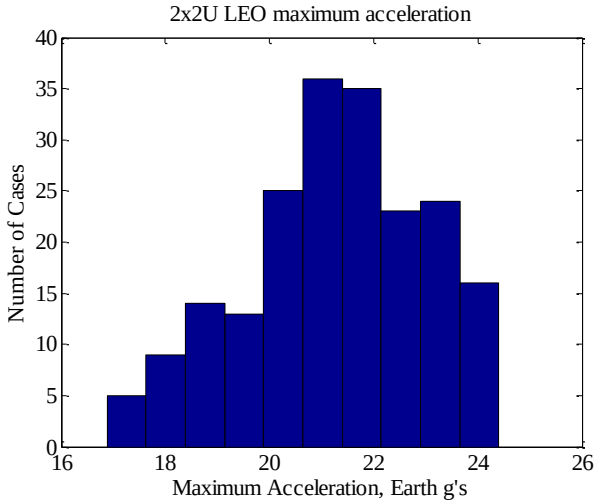

Figure 10 Ringslot Maximum Opening Deceleration Histogram

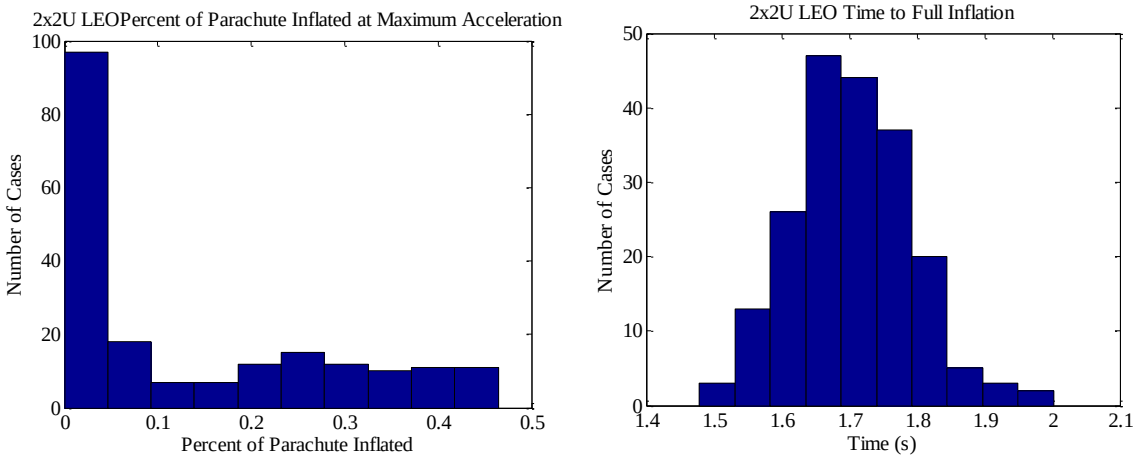

Figure 11 Ringslot Parachute Inflation Characteristics

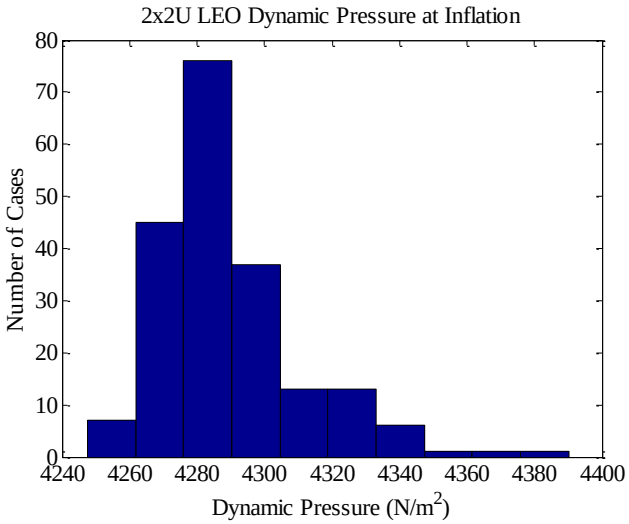

Figure 12 Ringslot Parachute Dynamic Pressure

Appendix B – Disk-Gap-Band Parachute Inflation Monte Carlo Results – 2x2U LEO

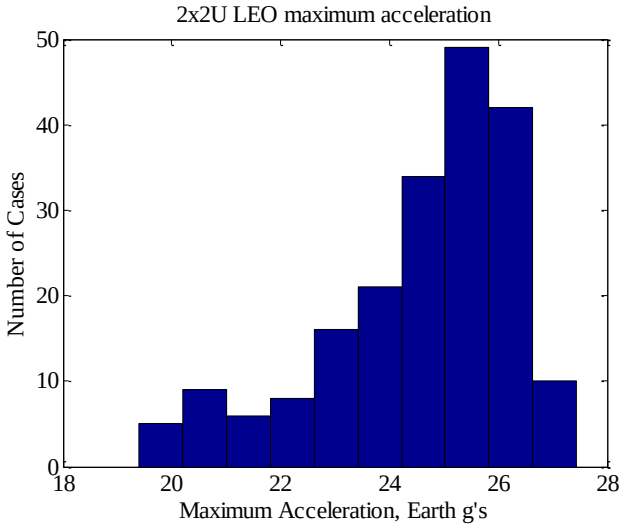

Figure 13 DGB Maximum Opening Deceleration Histogram

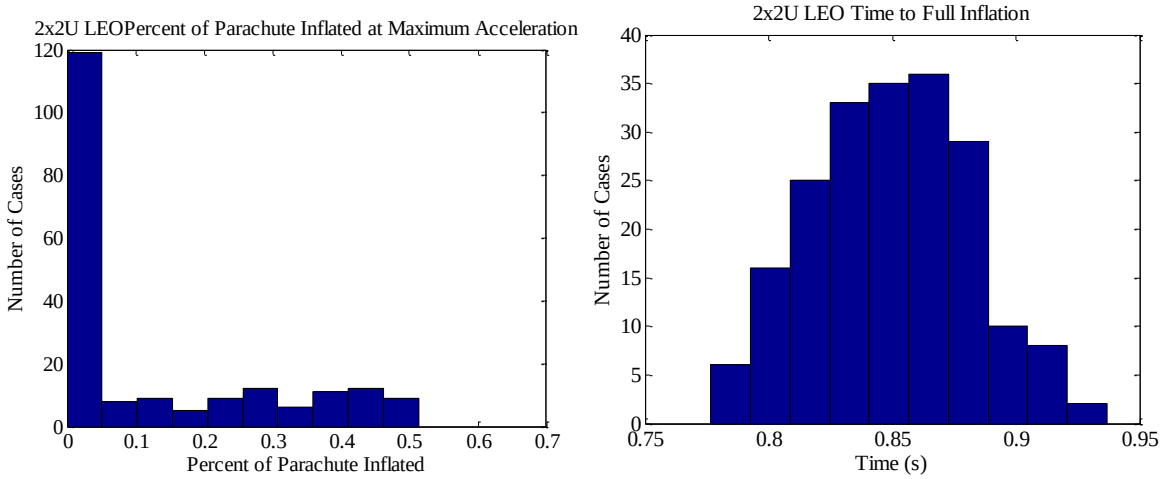

Figure 14 DGB Parachute Inflation Characteristics

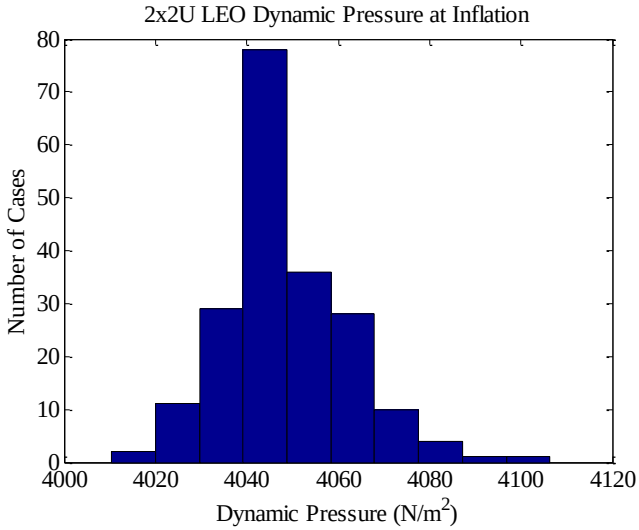

Figure 15 DGB Parachute Dynamic Pressure

Appendix C – Extended Skirt 14.3% Full Parachute Inflation Monte Carlo Results – 2x2U LEO

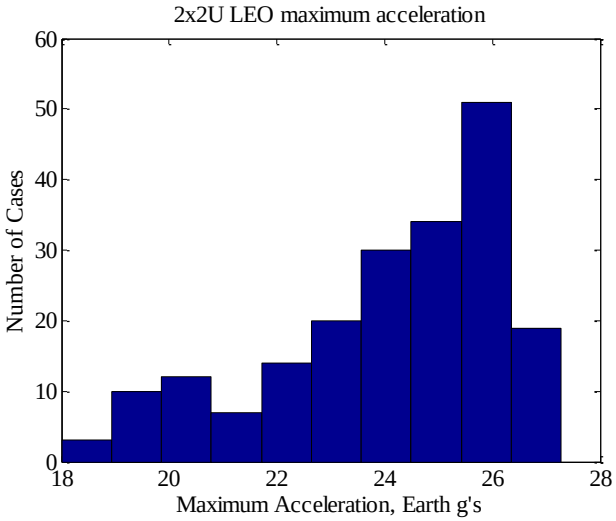

Figure 16 Extended Skirt 14.3% Maximum Opening Deceleration Histogram

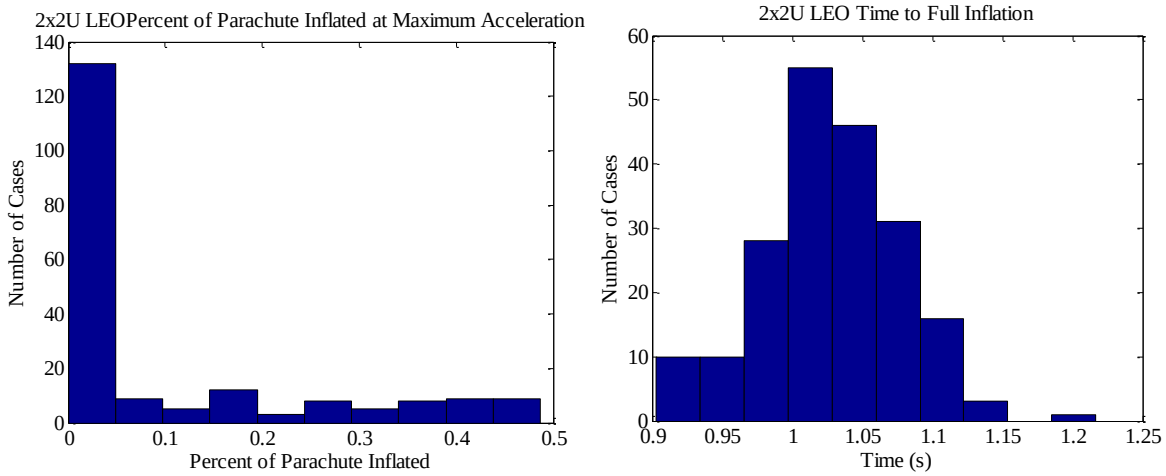

Figure 17 Extended Skirt 14.3% Parachute Inflation Characteristics

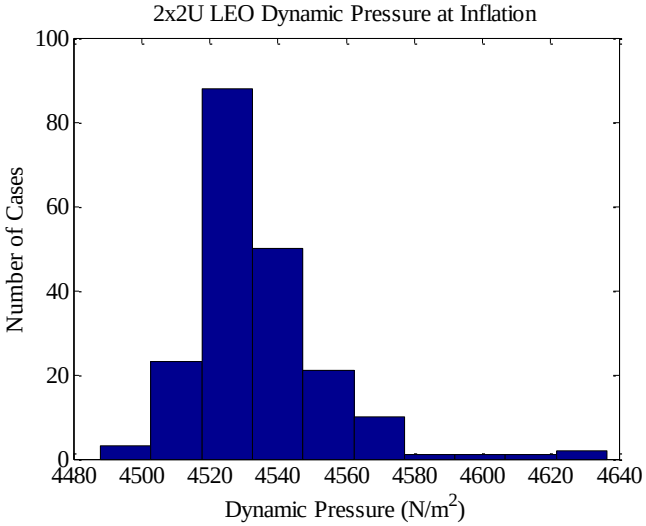

Figure 18 Extended Skirt 14.3% Parachute Dynamic Pressure

Appendix D – Conical Ribbon Parachute Inflation Monte Carlo Results – 2x2U LEO

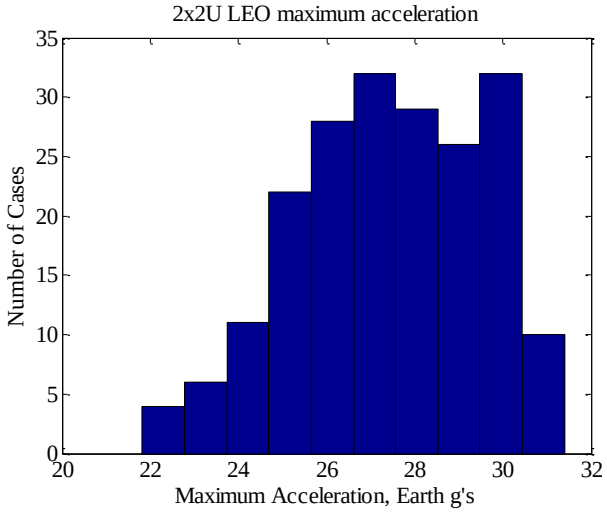

Figure 19 Conical Ribbon Maximum Opening Deceleration Histogram

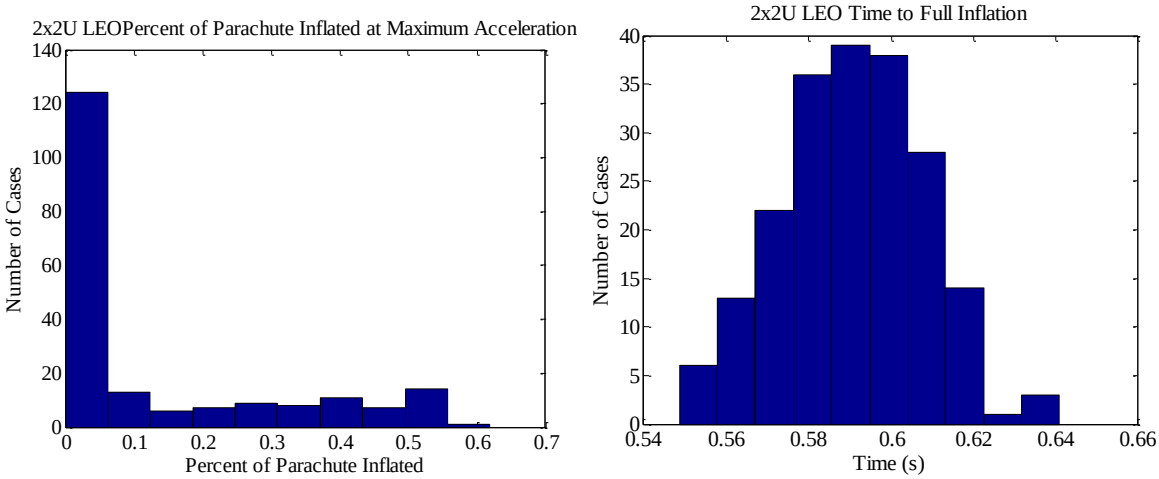

Figure 20 Conical Ribbon Parachute Inflation Characteristics

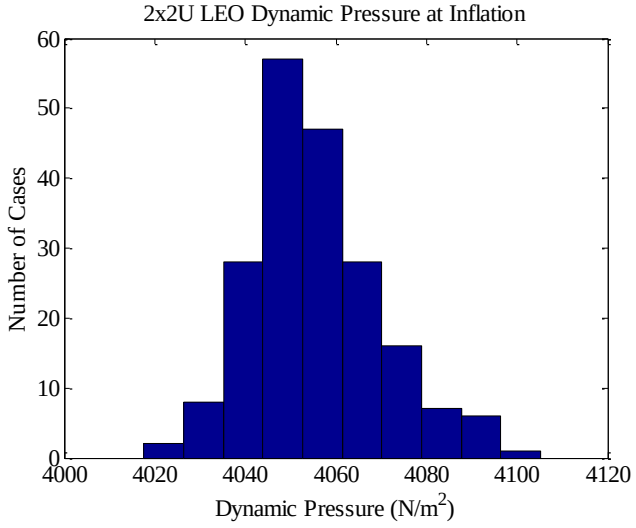

Figure 21 Conical Ribbon Parachute Dynamic Pressure

Appendix E - 2x2U LEO Impact Monte Carlo Results

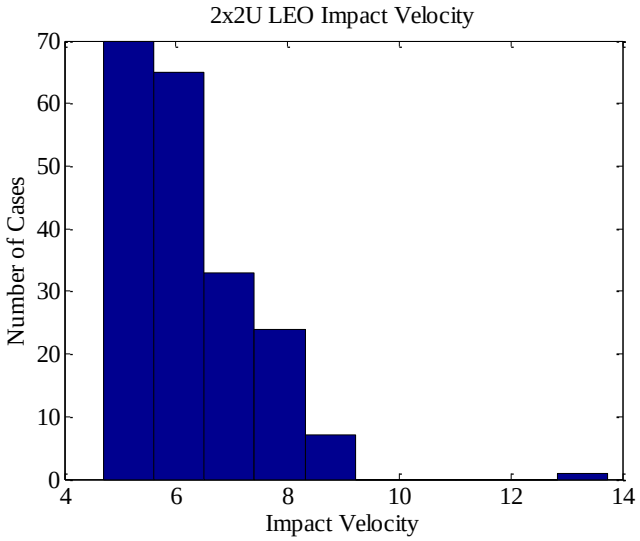

Figure 22 Ringslot Parachute Impact Velocity Histogram

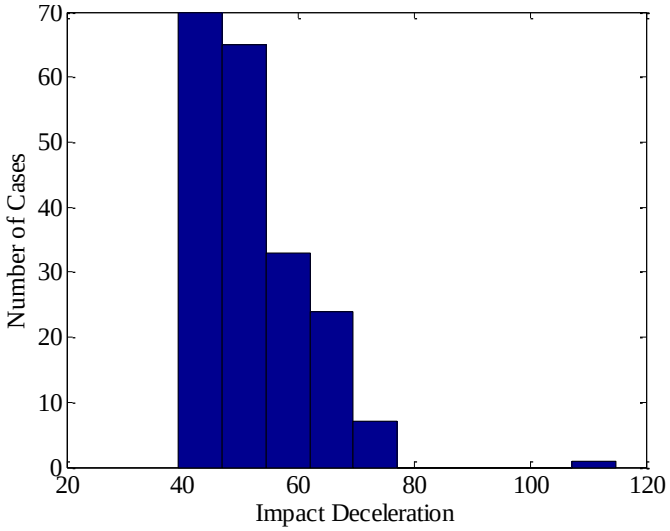

Figure 23 Ringslot Parachute Impact Deceleration Histogram (g)

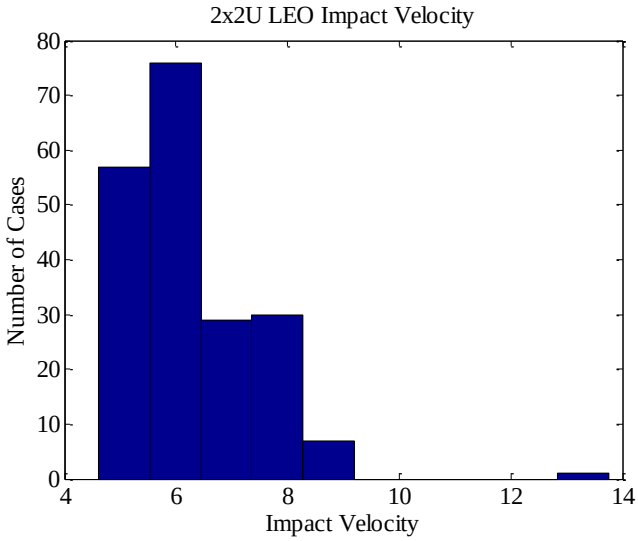

Figure 24 DGB Parachute Impact Velocity Histogram

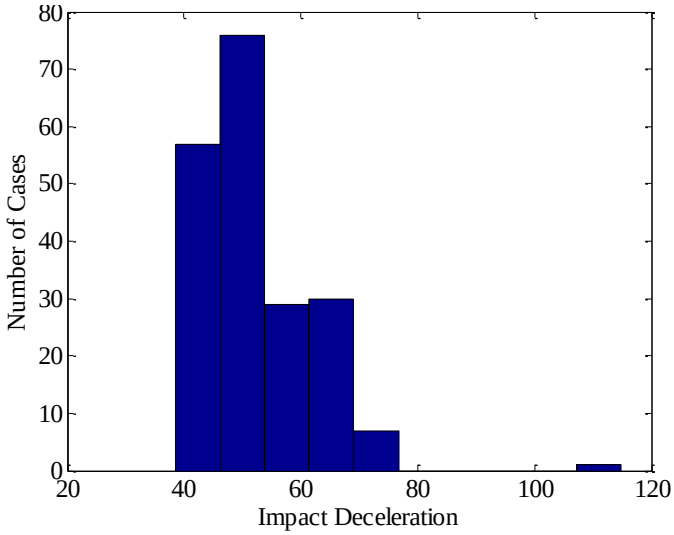

Figure 25 DGB Impact Deceleration Histogram (g)

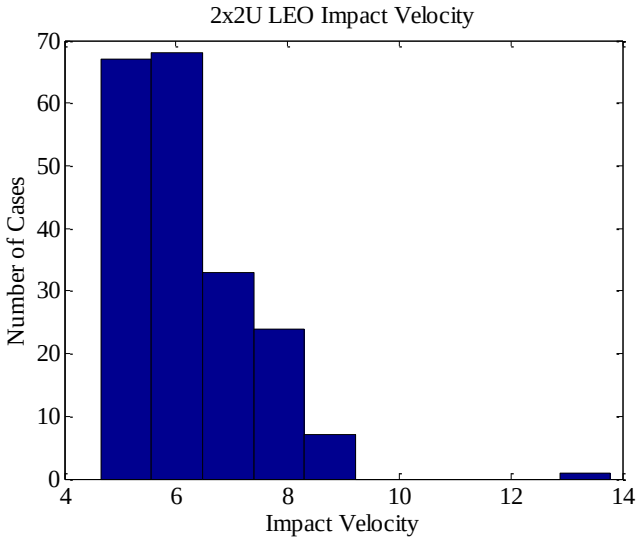

Figure 26 Extended Skirt 14.3% Parachute Impact Velocity Histogram

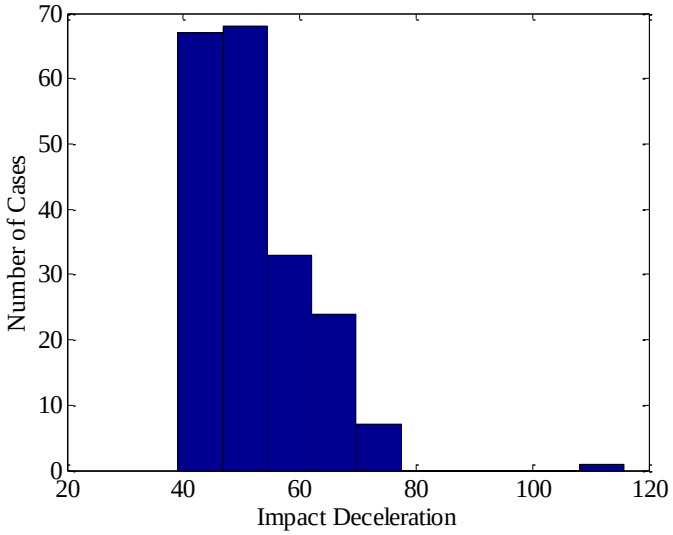

Figure 27 Extended Skirt 14.3% Parachute Impact Deceleration Histogram (g)

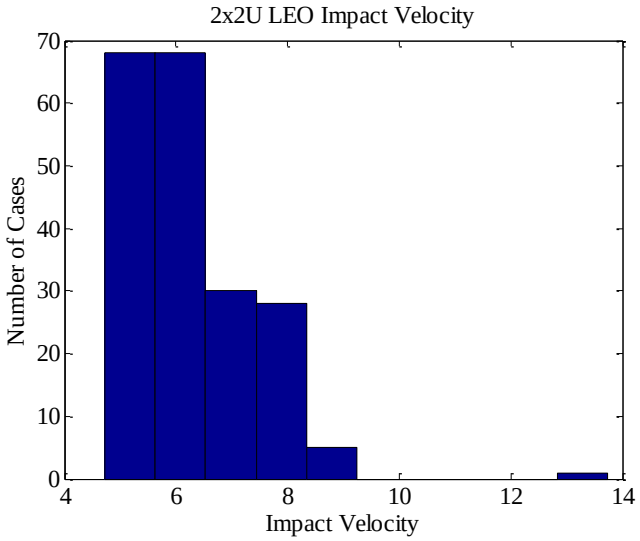

Figure 28 Conical Ribbon Parachute Impact Velocity Histogram

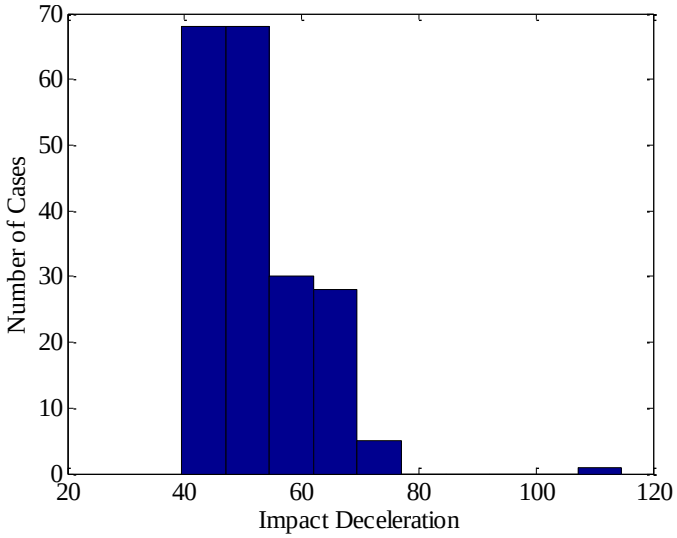

Figure 29 Conical Ribbon Parachute Impact Deceleration Histogram (g)

Appendix F – 1U LEO Monte Carlo Results, 100% Parachute Area

Conical

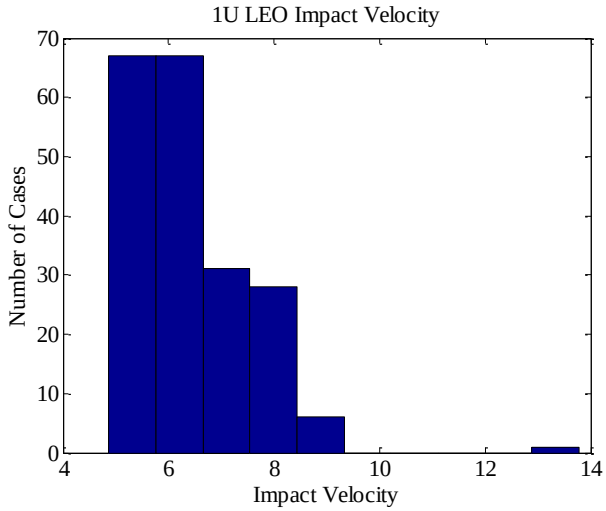

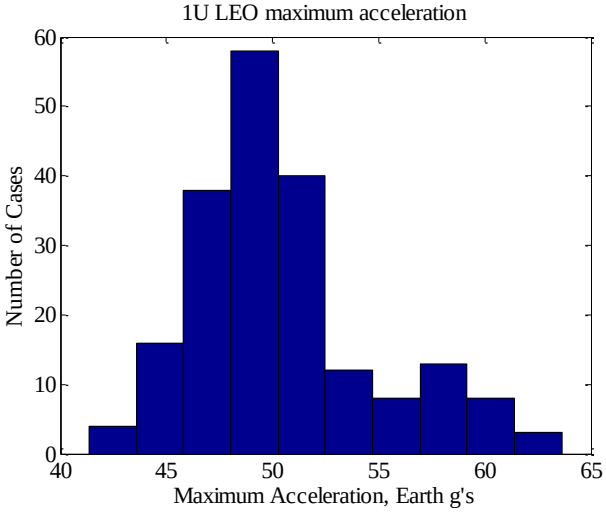

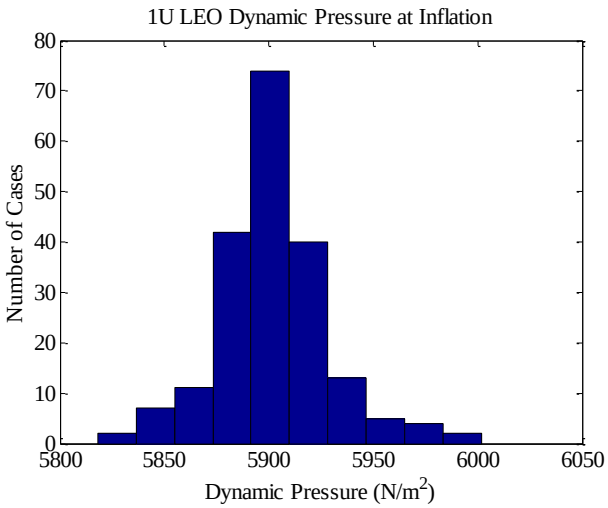

Biconical

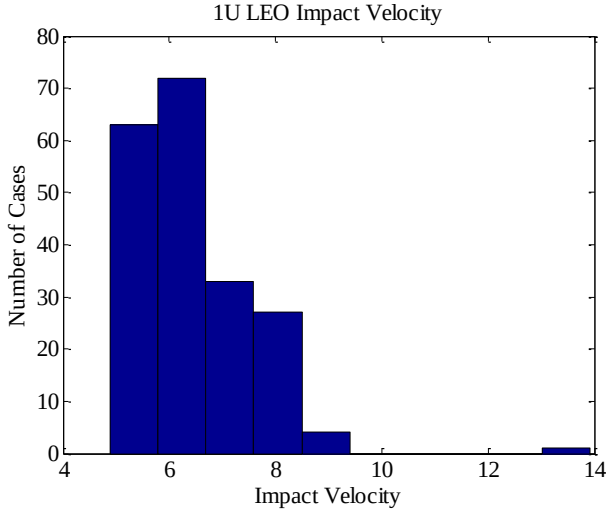

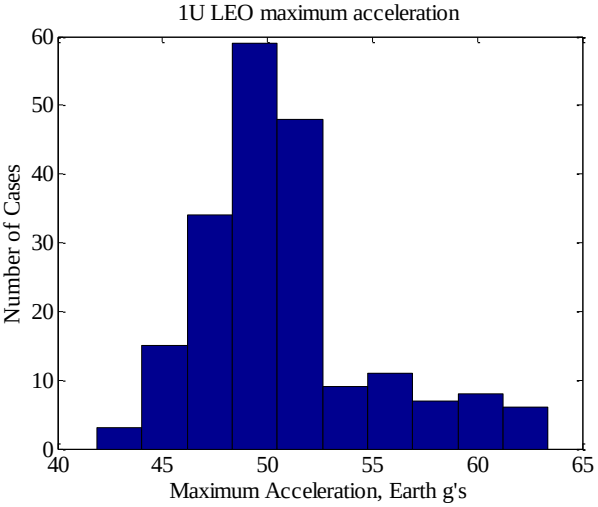

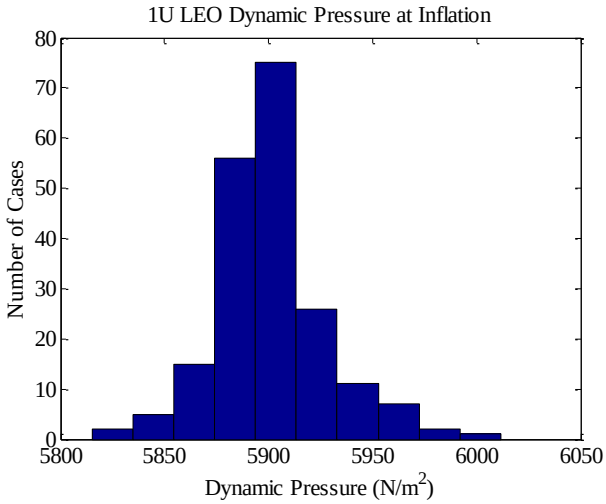
1U LEO Dynamic Pressure at Inflation
Number of Cases
Dynamic Pressure (N/m2)
0
10
20
30
40
50
60
70
80
5800
5850
5900
5950
6000
6050

Triconical

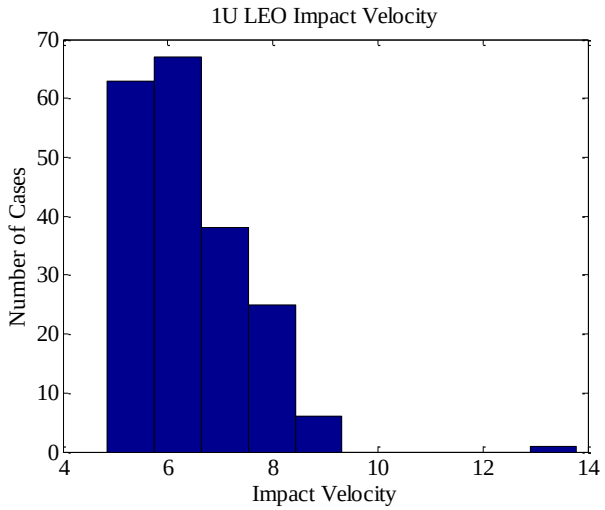
1U LEO Impact Velocity
Number of Cases
Impact Velocity
0
10
20
30
40
50
60
70
4
6
8
10
12
14

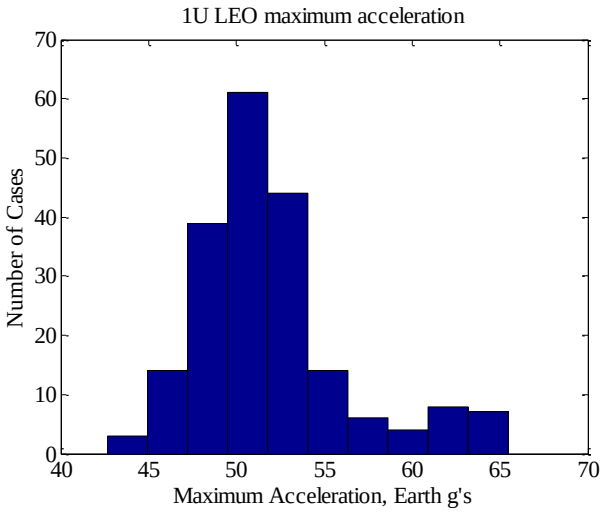
1U LEO maximum acceleration
Number of Cases
Maximum Acceleration, Earth g's
0
10
20
30
40
50
60
70
40
45
50
55
60
65
70

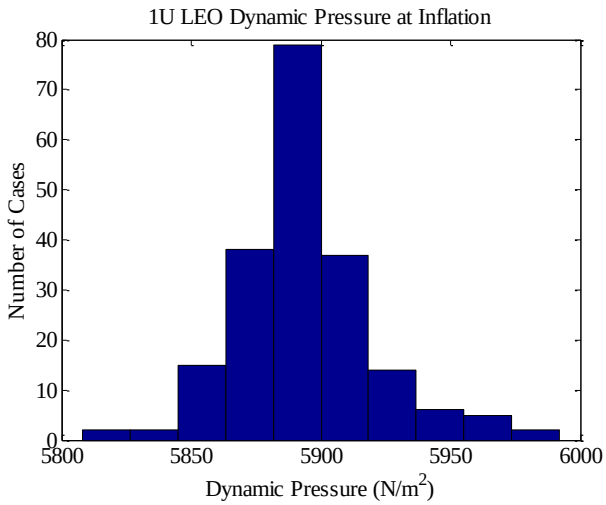
1U LEO Dynamic Pressure at Inflation
Number of Cases
Dynamic Pressure (N/m2)
0
10
20
30
40
50
60
70
80
5800
5850
5900
5950
6000

Extended Skirt 10% Flat

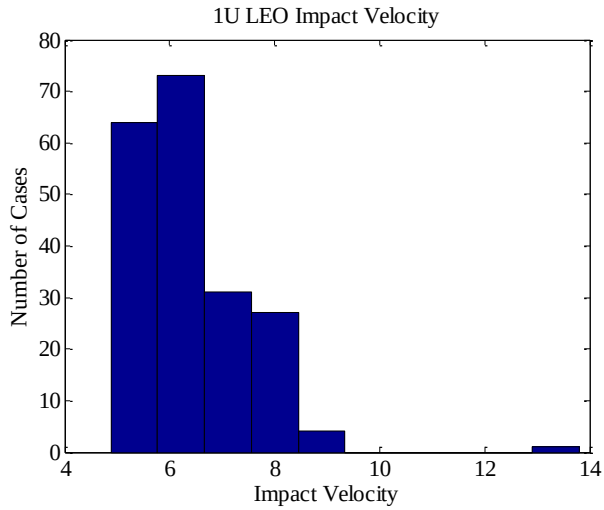

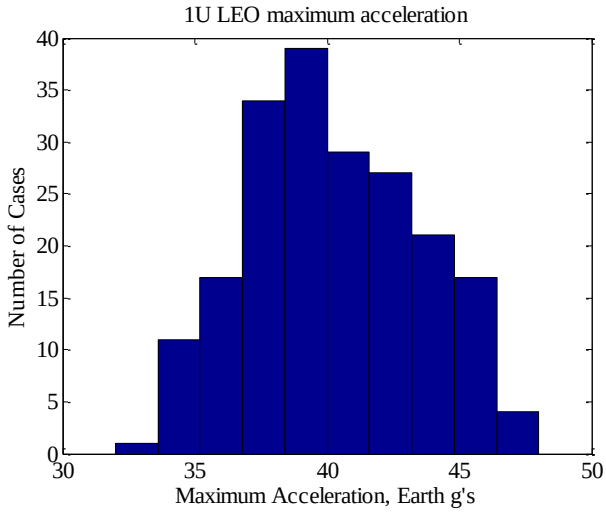

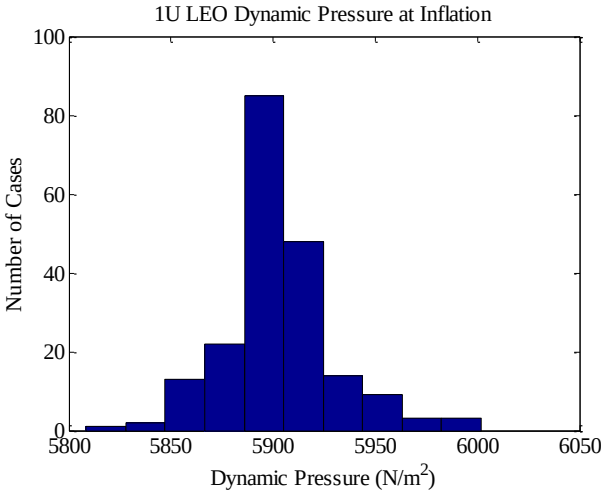

Extended Skirt 14.3% Full

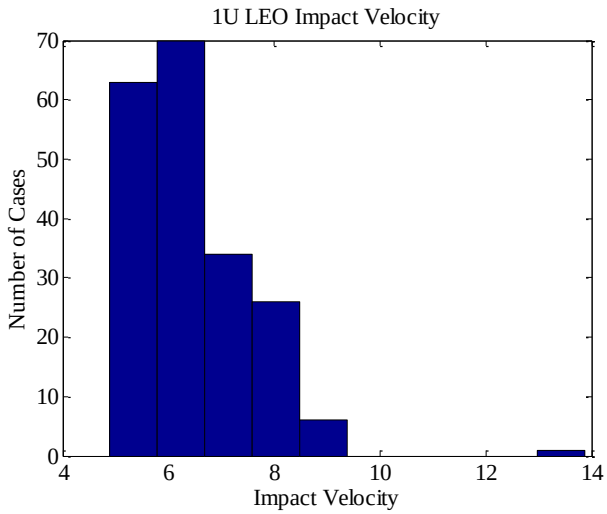

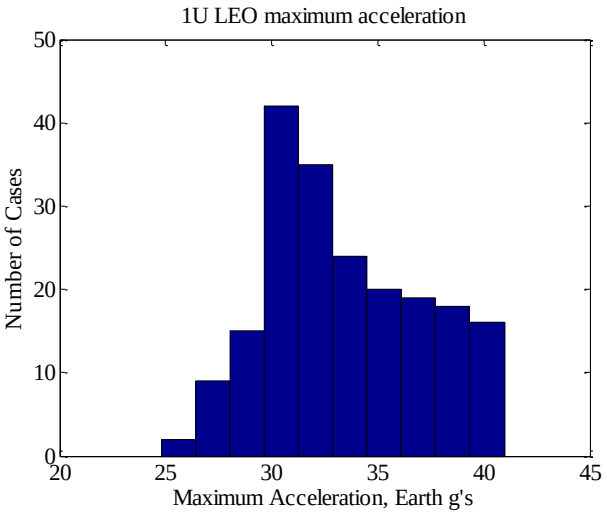

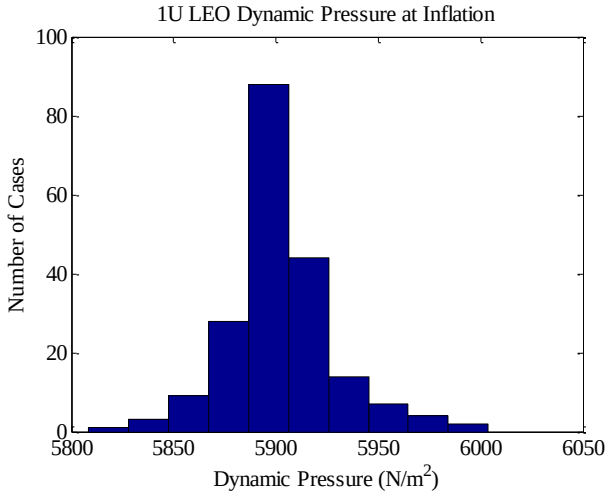
1U LEO Dynamic Pressure at Inflation
Number of Cases
Dynamic Pressure (N/m2)
0
20
40
60
80
100
5800
5850
5900
5950
6000
6050

Annular

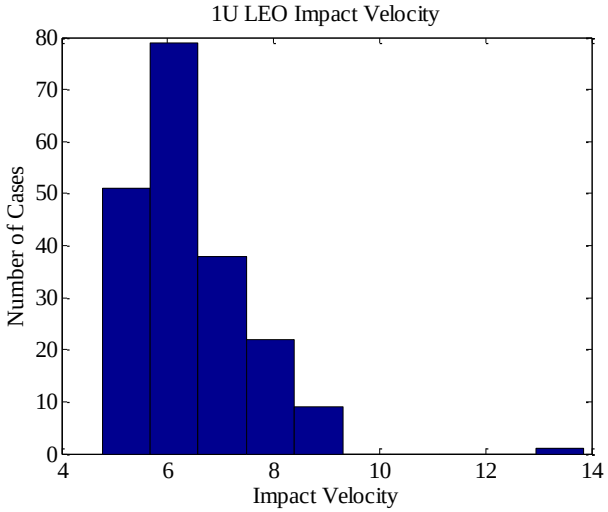
1U LEO Impact Velocity
Number of Cases
Impact Velocity
0
10
20
30
40
50
60
70
80
4
6
8
10
12
14

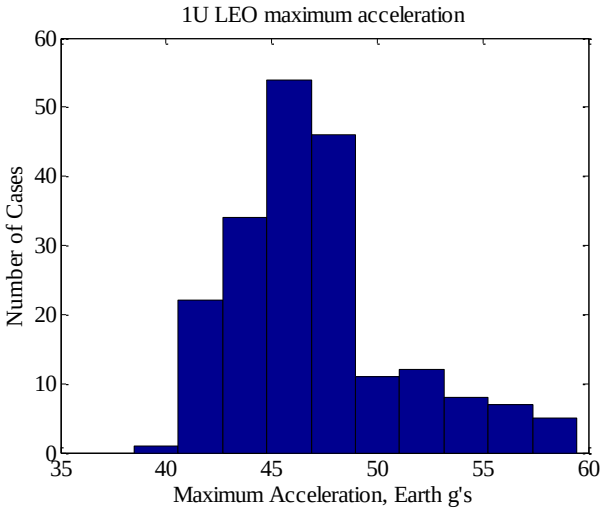
1U LEO maximum acceleration
Number of Cases
Maximum Acceleration, Earth g's
0
10
20
30
40
50
60
35
40
45
50
55
60

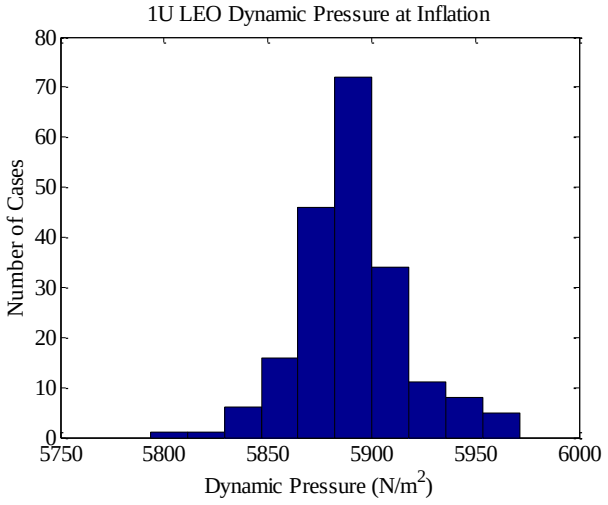
1U LEO Dynamic Pressure at Inflation
Number of Cases
Dynamic Pressure (N/m2)
0
10
20
30
40
50
60
70
80
5750
5800
5850
5900
5950
6000

Cross

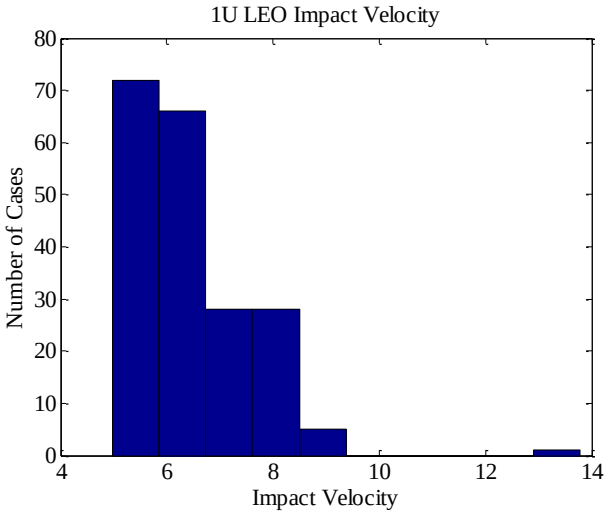

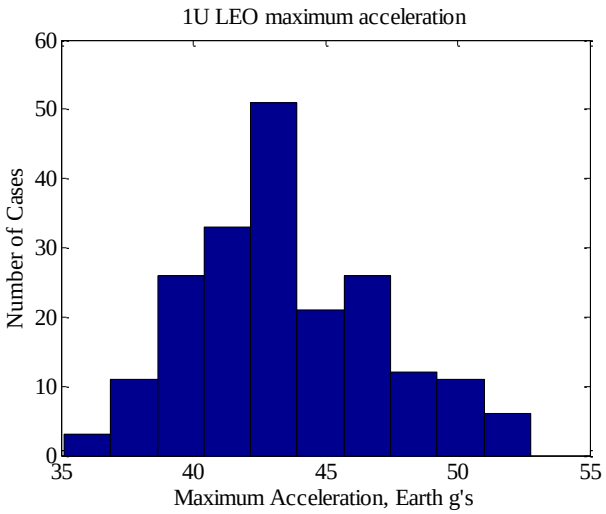

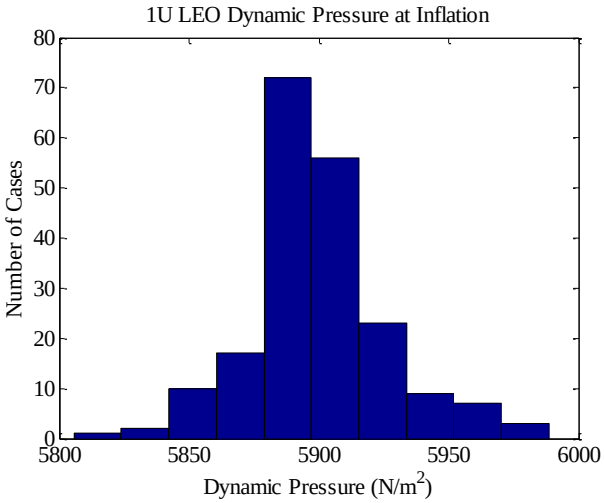

Conical Ribbon

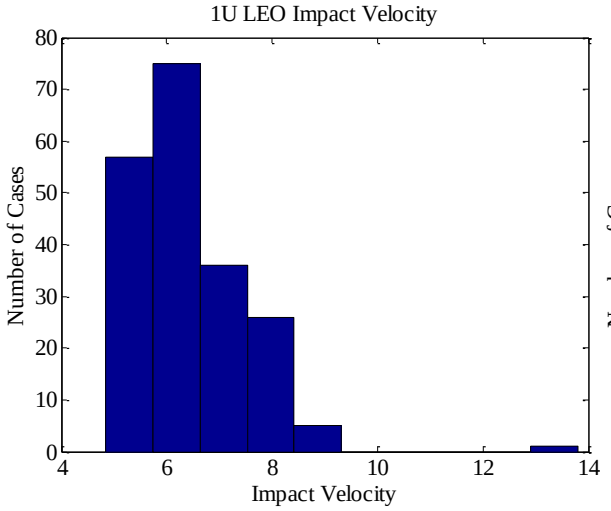

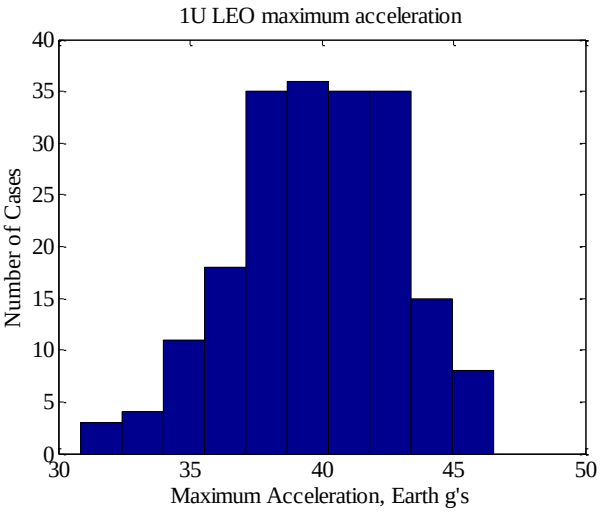

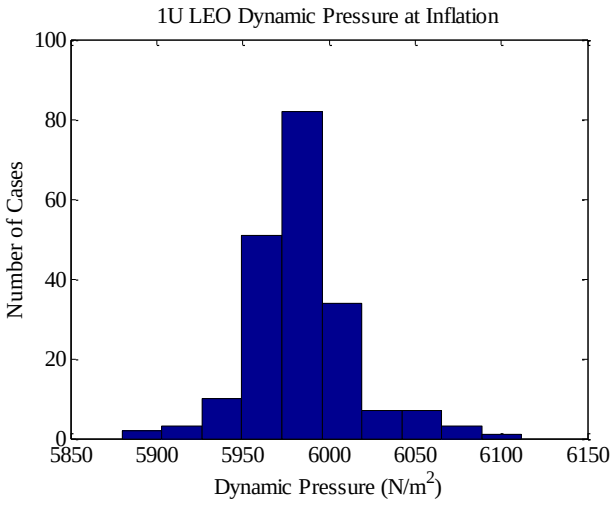
1U LEO Dynamic Pressure at Inflation
Number of Cases
Dynamic Pressure (N/m2)
0
20
40
60
80
100
5850
5900
5950
6000
6050
6100
6150

Ringslot

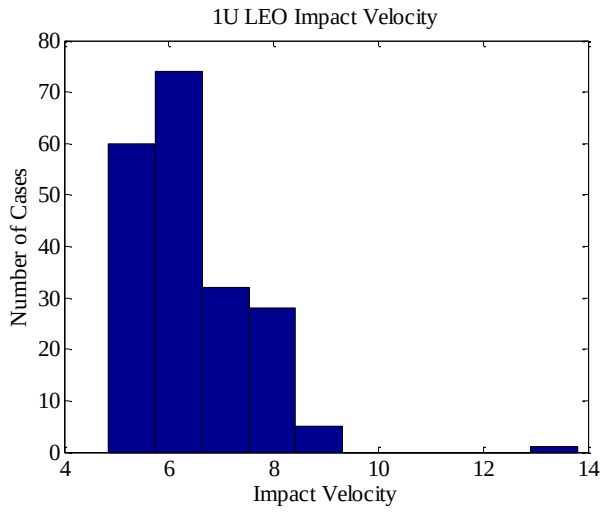
1U LEO Impact Velocity
Number of Cases
Impact Velocity
0
10
20
30
40
50
60
70
80
4
6
8
10
12
14

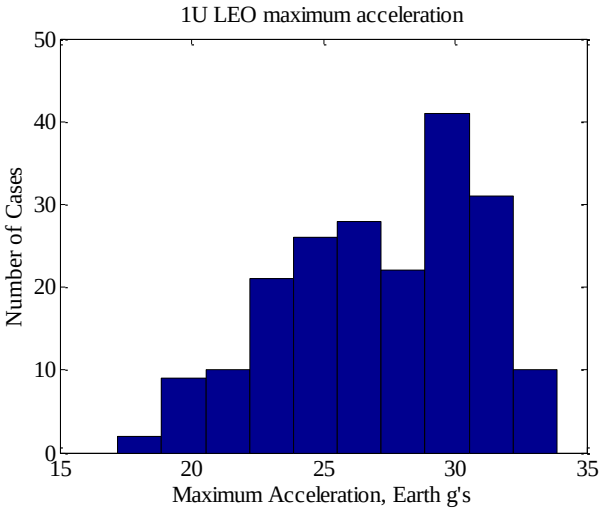
1U LEO maximum acceleration
Number of Cases
Maximum Acceleration, Earth g's
0
10
20
30
40
50
15
20
25
30
35

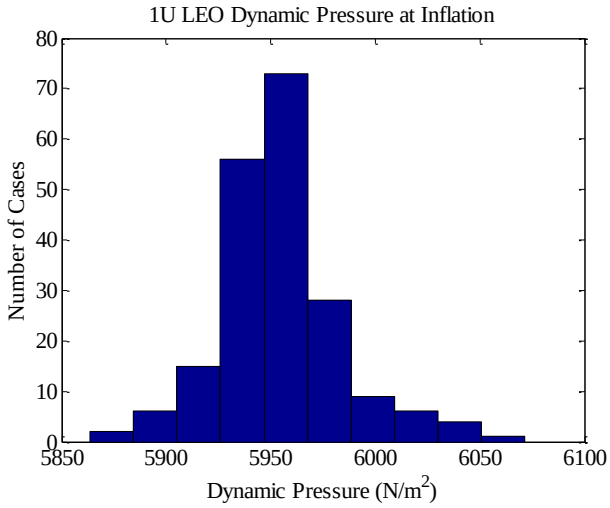
1U LEO Dynamic Pressure at Inflation
Number of Cases
Dynamic Pressure (N/m2)
0
10
20
30
40
50
60
70
80
5850
5900
5950
6000
6050
6100

Ringsail

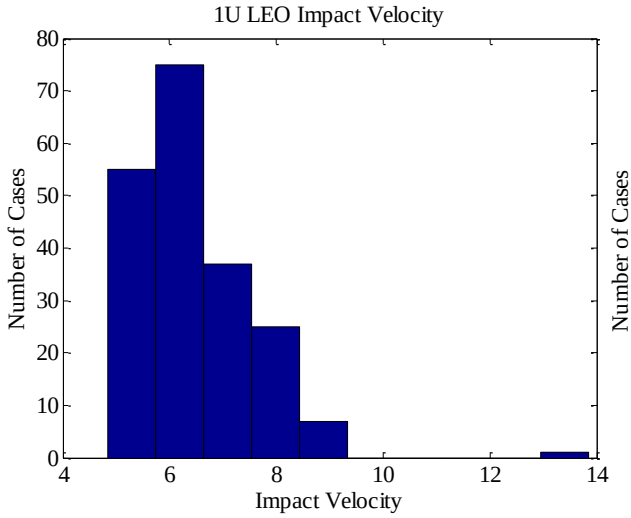
1U LEO Impact Velocity
Number of Cases
Impact Velocity
0
10
20
30
40
50
60
70
80
4
6
8
10
12
14

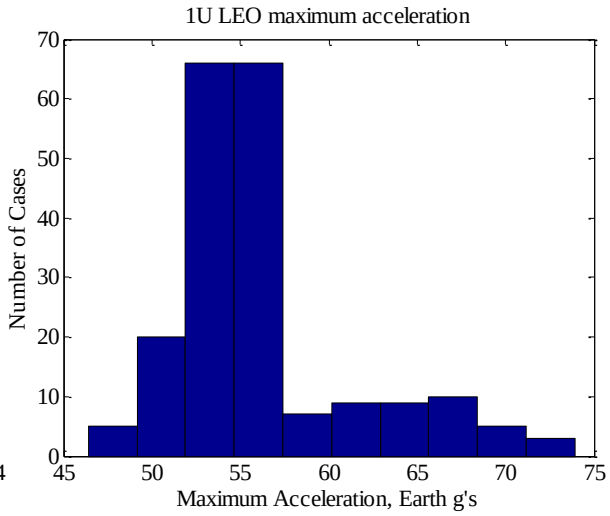
1U LEO maximum acceleration
Number of Cases
Maximum Acceleration, Earth g's
0
10
20
30
40
50
60
70
45
50
55
60
65
70
75

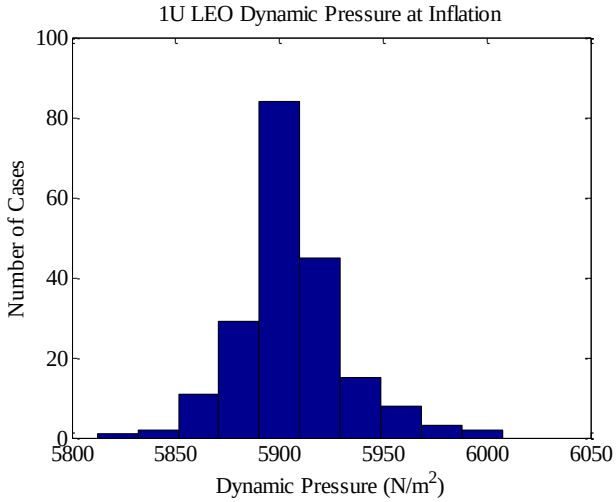
1U LEO Dynamic Pressure at Inflation
Number of Cases
Dynamic Pressure (N/m2)
0
20
40
60
80
100
5800
5850
5900
5950
6000
6050

Disk-Gap-Band

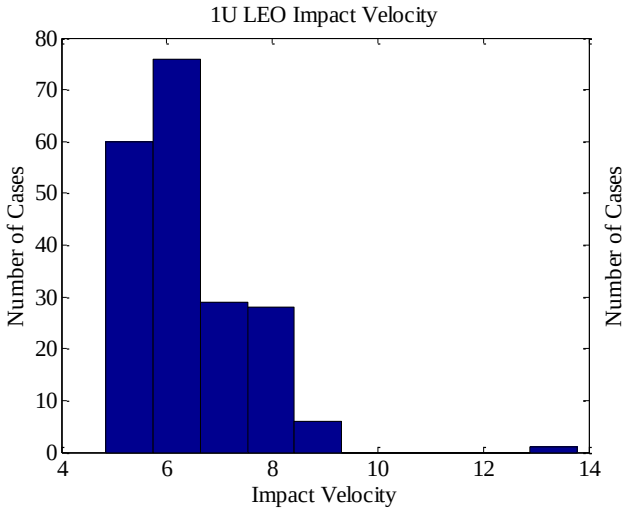

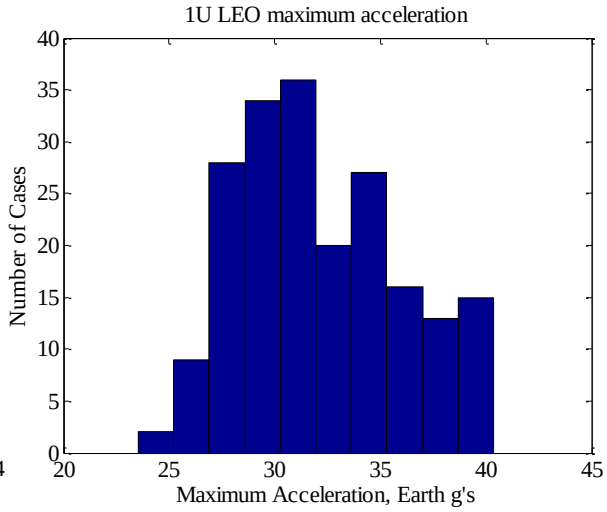

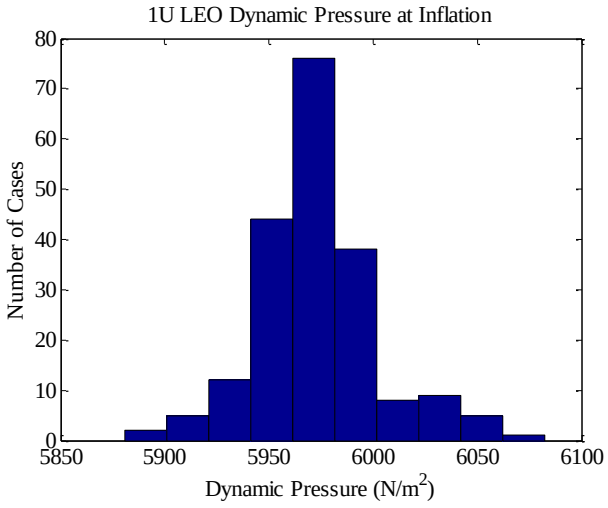

Appendix G – 1U LEO Monte Carlo Results, 300% Parachute Area

Conical

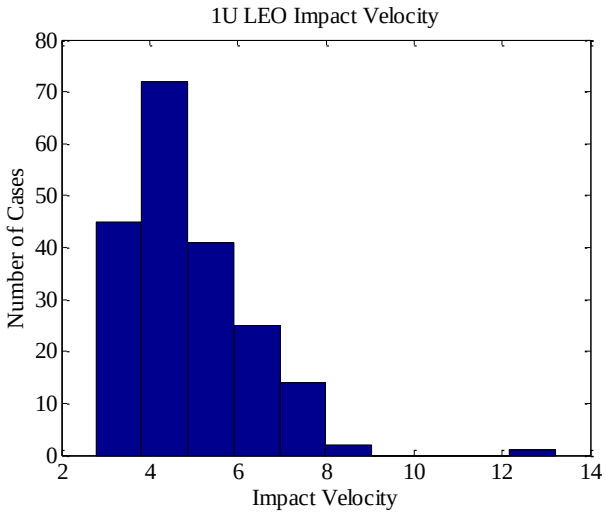

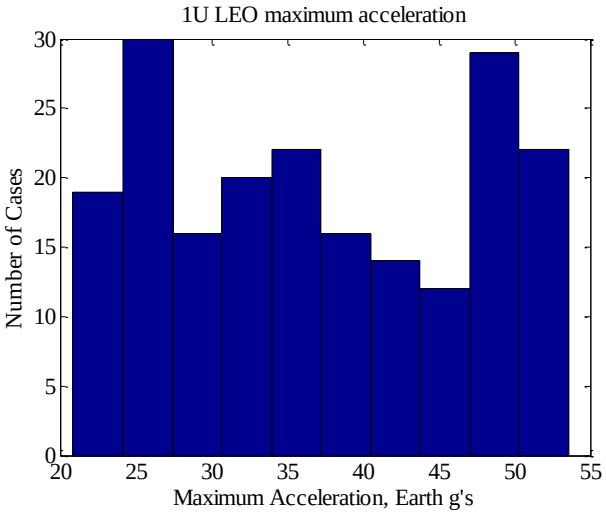

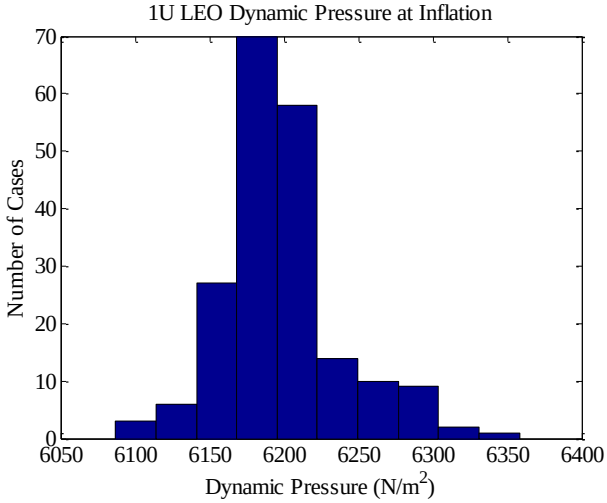

Biconical

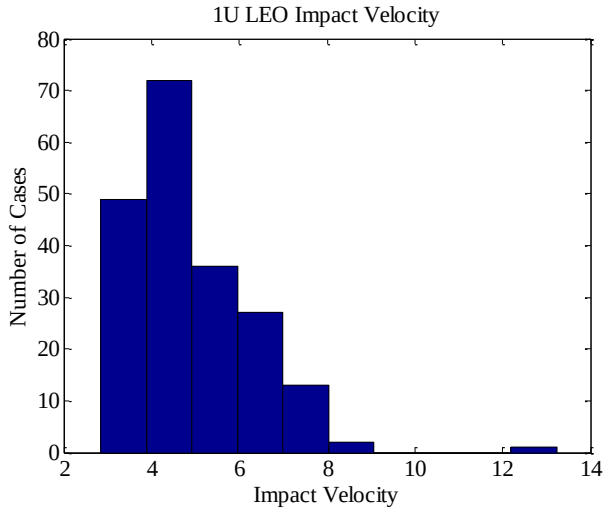

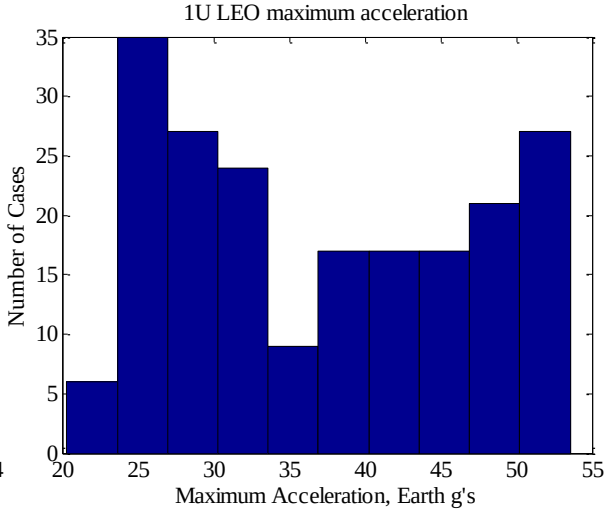

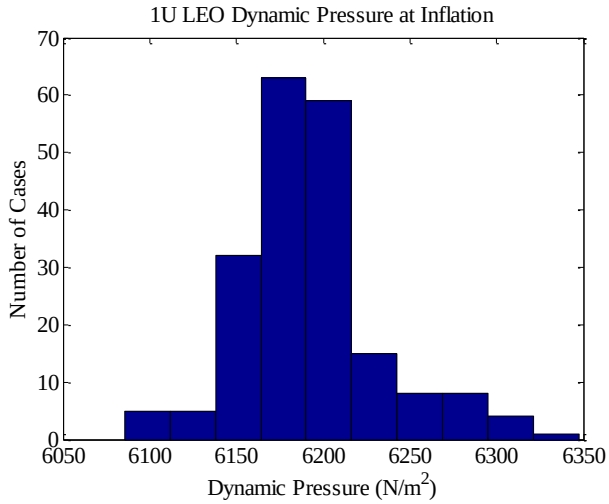
1U LEO Dynamic Pressure at Inflation
Number of Cases
Dynamic Pressure (N/m2)
0
10
20
30
40
50
60
70
6050
6100
6150
6200
6250
6300
6350

Triconical

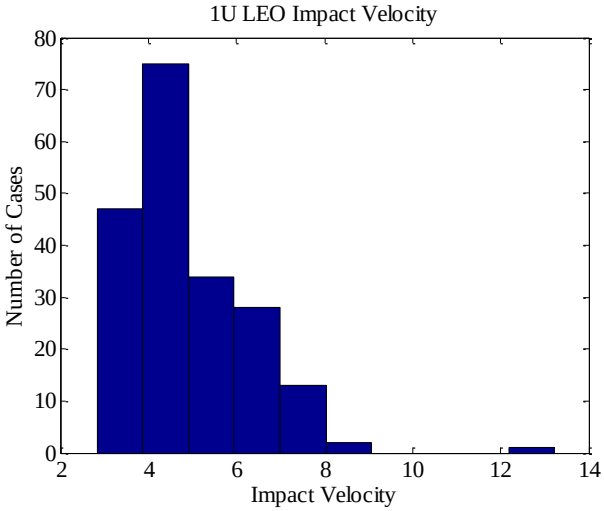
1U LEO Impact Velocity
Number of Cases
Impact Velocity
0
10
20
30
40
50
60
70
80
2
4
6
8
10
12
14

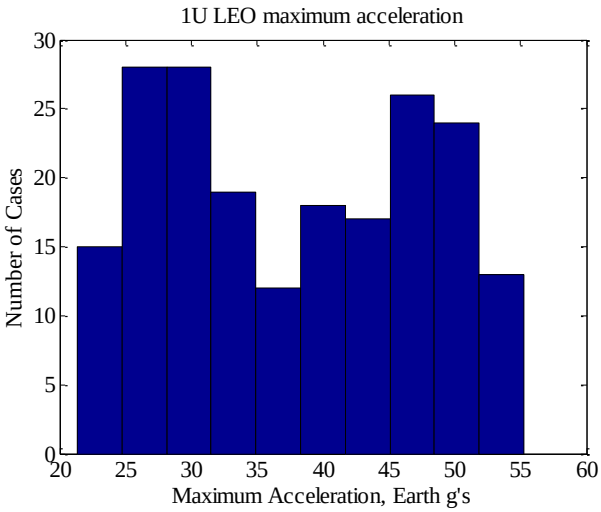
1U LEO maximum acceleration
Number of Cases
Maximum Acceleration, Earth g's
0
5
10
15
20
25
30
20
25
30
35
40
45
50
55
60

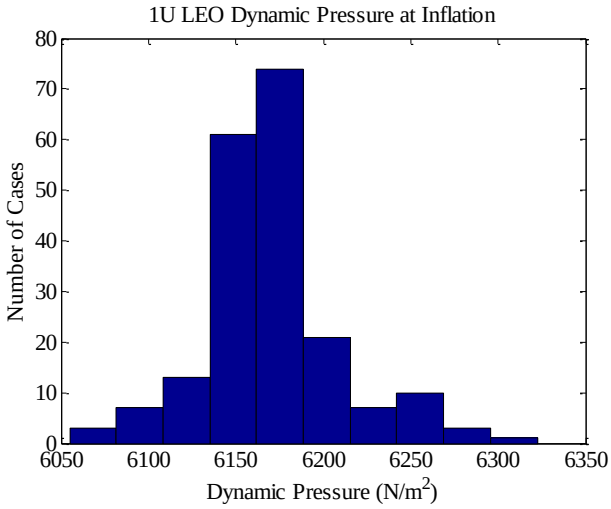
1U LEO Dynamic Pressure at Inflation
Number of Cases
Dynamic Pressure (N/m2)
0
10
20
30
40
50
60
70
80
6050
6100
6150
6200
6250
6300
6350

Extended Skirt 10% Flat

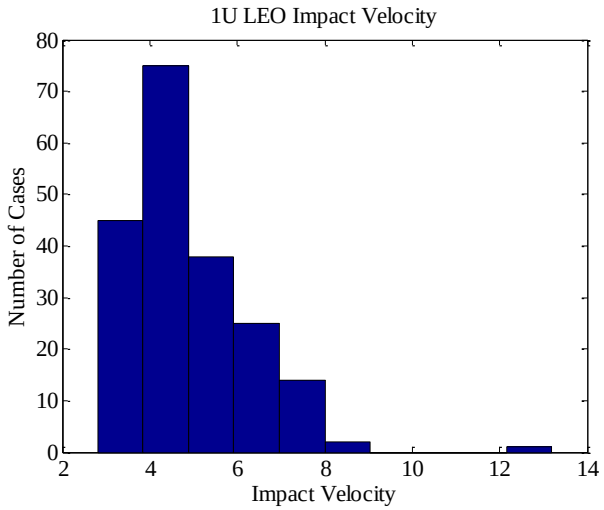

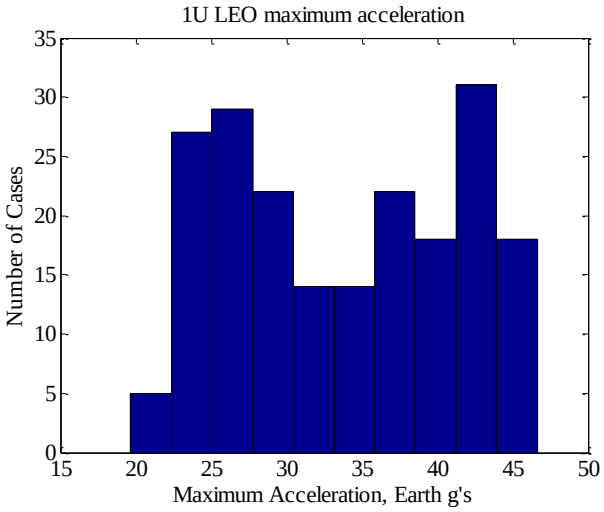

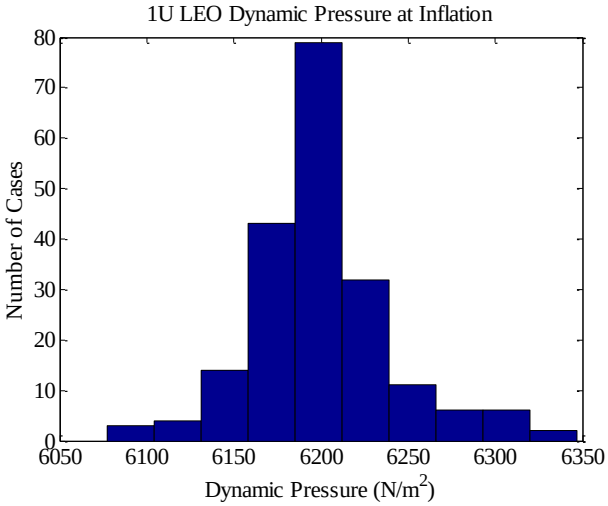

Extended Skirt 14.3% Full

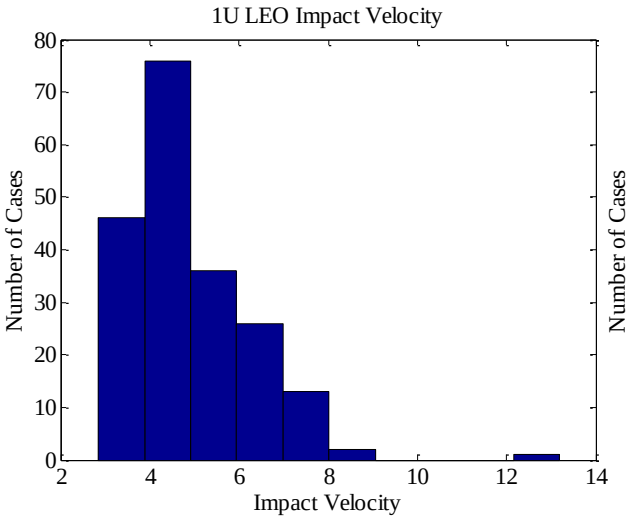

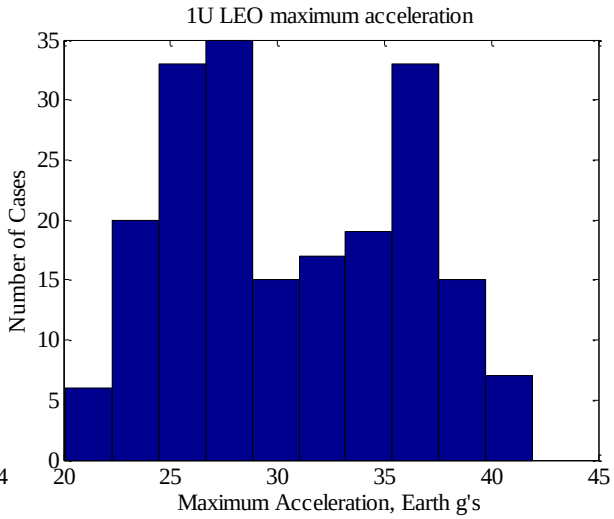

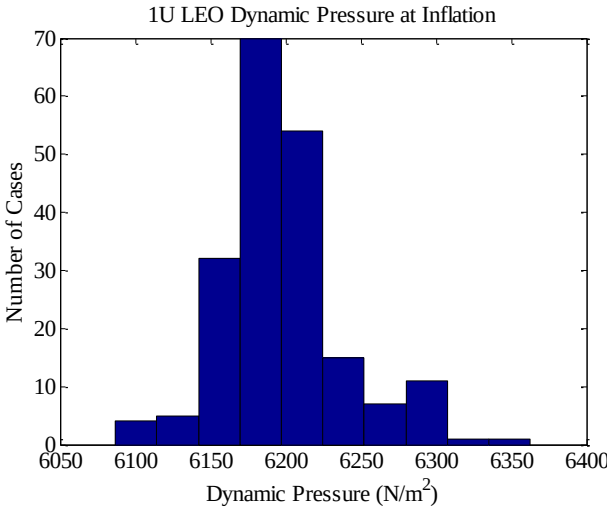
1U LEO Dynamic Pressure at Inflation
Number of Cases
Dynamic Pressure (N/m2)
0
10
20
30
40
50
60
70
6050
6100
6150
6200
6250
6300
6350
6400

Annular

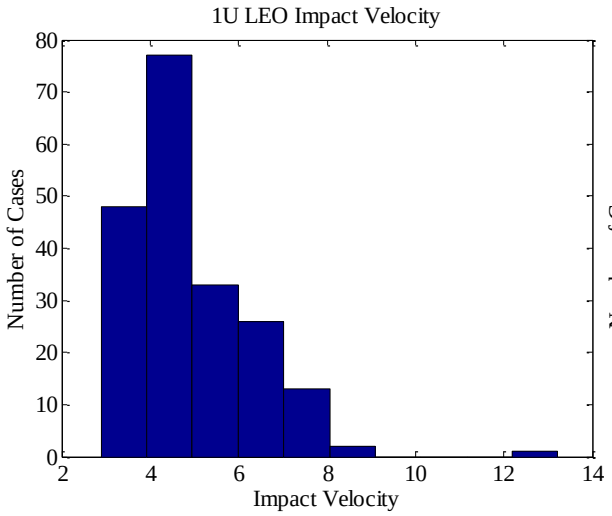
1U LEO Impact Velocity
Number of Cases
Impact Velocity
0
10
20
30
40
50
60
70
80
2
4
6
8
10
12
14

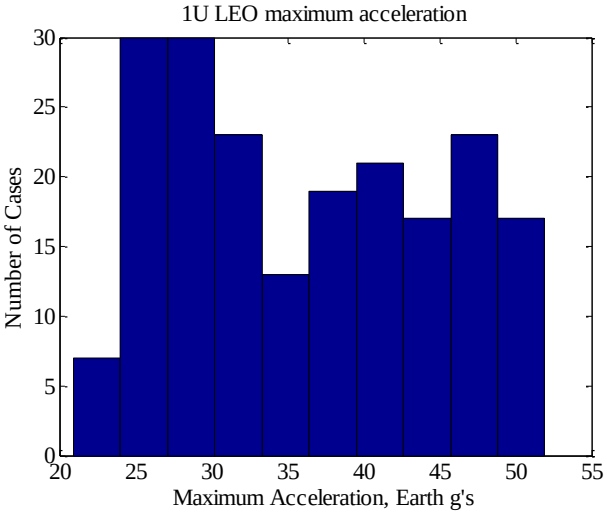
1U LEO maximum acceleration
Number of Cases
Maximum Acceleration, Earth g's
0
5
10
15
20
25
30
20
25
30
35
40
45
50
55

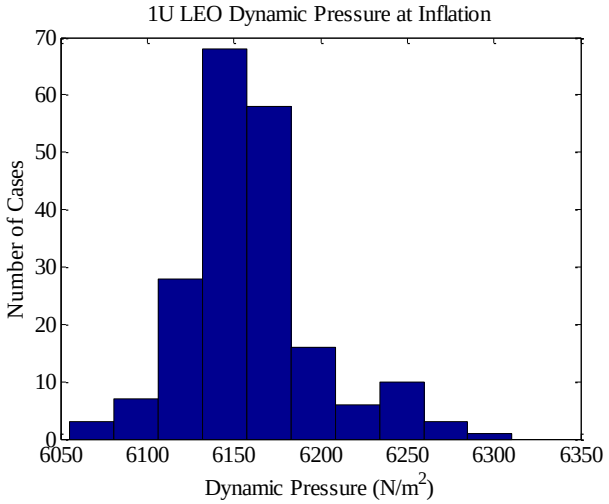
1U LEO Dynamic Pressure at Inflation
Number of Cases
Dynamic Pressure (N/m2)
0
10
20
30
40
50
60
70
6050
6100
6150
6200
6250
6300
6350

Cross

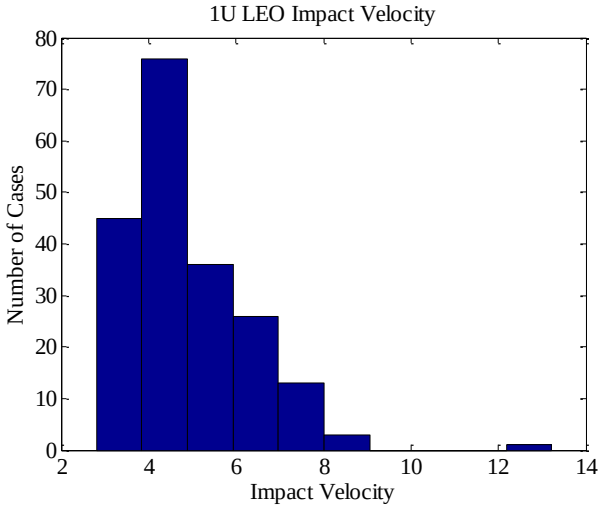

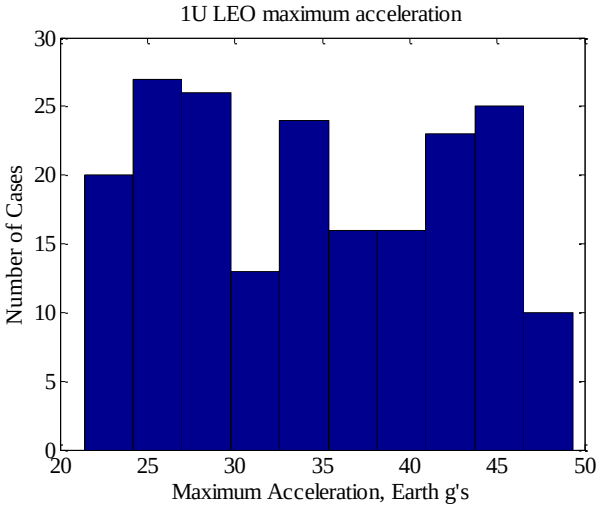

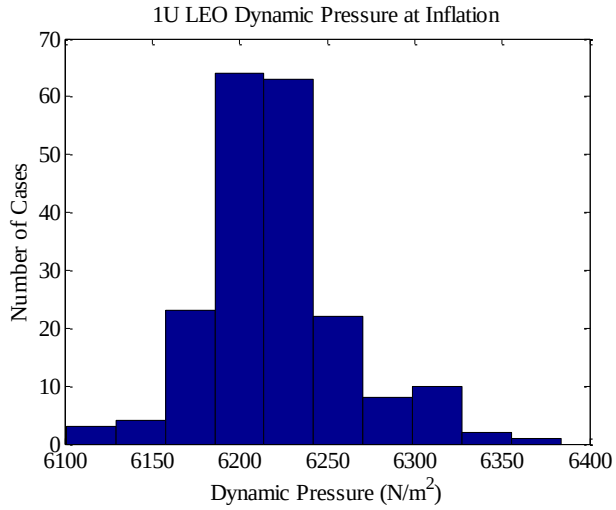

Conical Ribbon

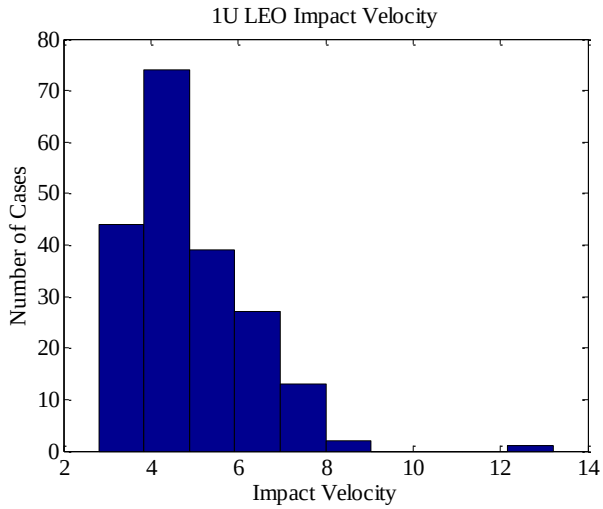

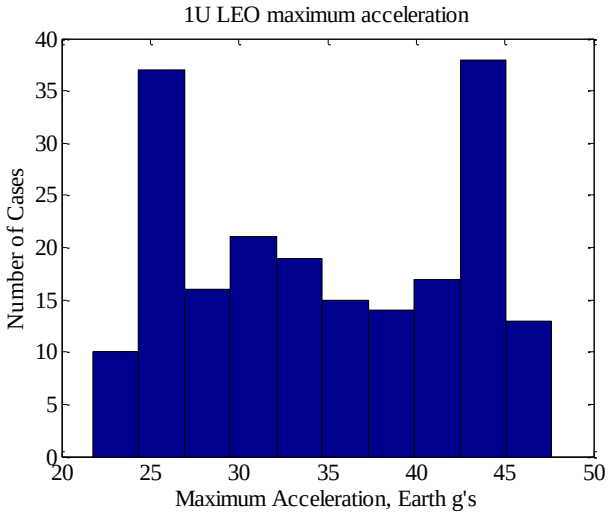

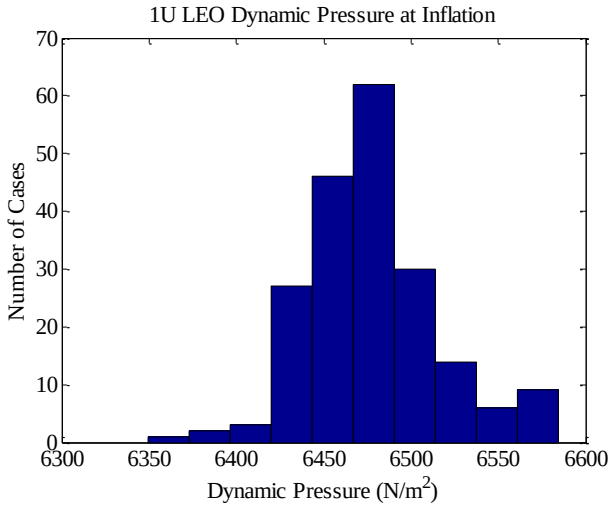
1U LEO Dynamic Pressure at Inflation
Number of Cases
Dynamic Pressure (N/m2)
0
10
20
30
40
50
60
70
6300
6350
6400
6450
6500
6550
6600

Ringslot

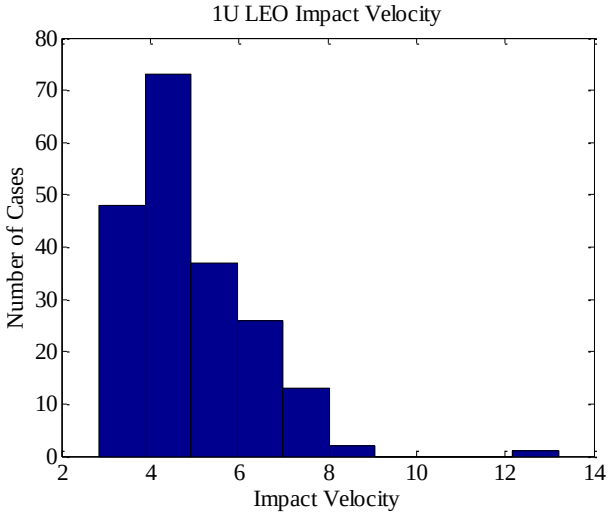
1U LEO Impact Velocity
Number of Cases
Impact Velocity
0
10
20
30
40
50
60
70
80
2
4
6
8
10
12
14

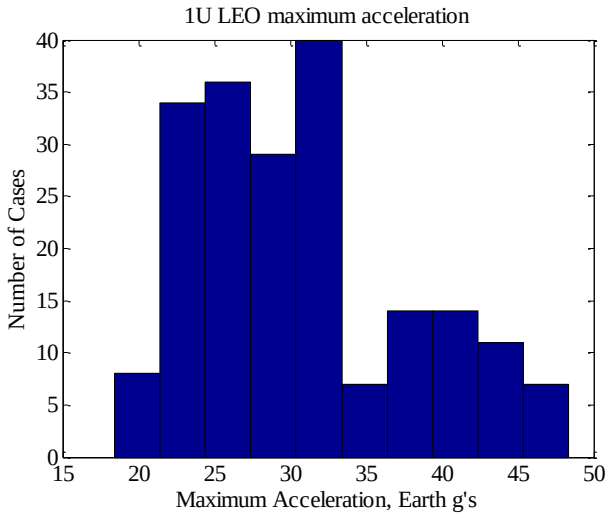
1U LEO maximum acceleration
Number of Cases
Maximum Acceleration, Earth g's
0
5
10
15
20
25
30
35
40
15
20
25
30
35
40
45
50

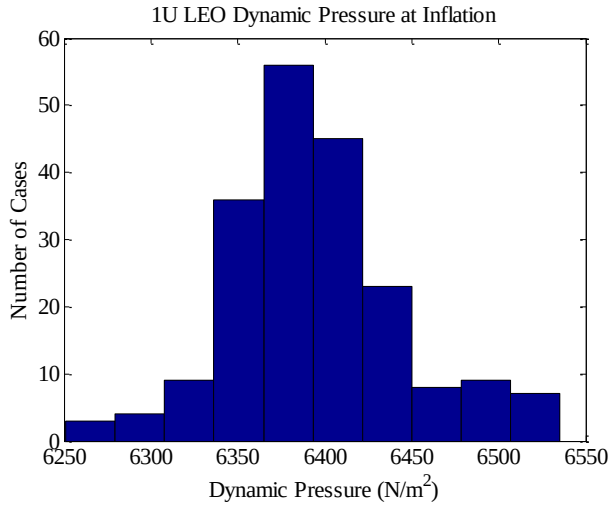
1U LEO Dynamic Pressure at Inflation
Number of Cases
Dynamic Pressure (N/m2)
0
10
20
30
40
50
60
6250
6300
6350
6400
6450
6500
6550

Ringsail

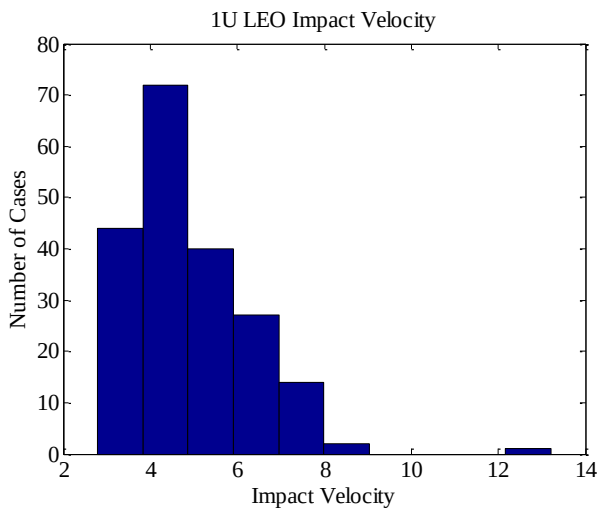
1U LEO Impact Velocity
Number of Cases
Impact Velocity
0
10
20
30
40
50
60
70
80
2
4
6
8
10
12
14

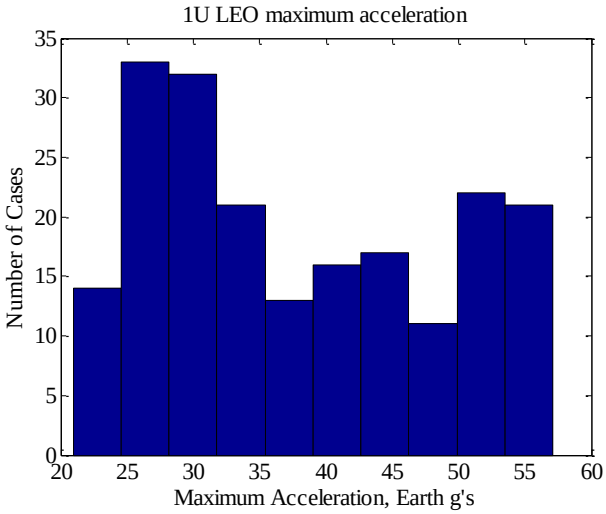
1U LEO maximum acceleration
Number of Cases
Maximum Acceleration, Earth g's
0
5
10
15
20
25
30
35
20
25
30
35
40
45
50
55
60

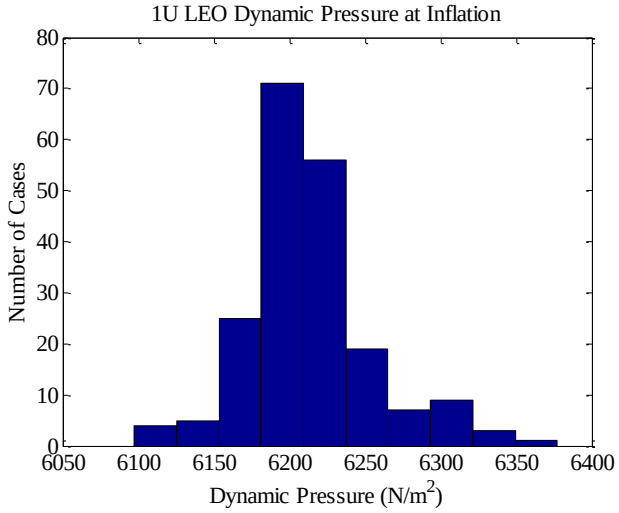
1U LEO Dynamic Pressure at Inflation
Number of Cases
Dynamic Pressure (N/m2)
0
10
20
30
40
50
60
70
80
6050
6100
6150
6200
6250
6300
6350
6400

Disk-Gap-Band